UNIVERSITÀ DEGLI STUDI DI PADOVA

DIPARTIMENTO DI BIOLOGIA

Corso di Laurea magistrale in Molecular Biology

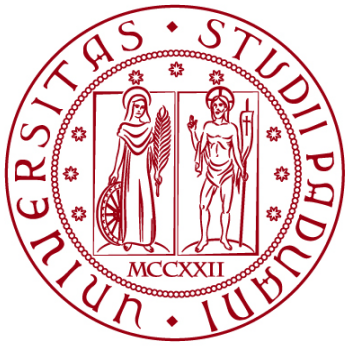

TESI DI LAUREA

Study of the role of the lncRNA *LADON* in melanoma tumour progression

Relatore: Prof. Francesco Argenton
Dipartimento di Biologia

Correlatore: Prof. Domenico Flagiello
Struttura: UMR7592 Institute Jacques Monod

Laureando: Nazareno Bisson

ANNO ACCADEMICO 2024/2025

Table of Contents

Abstract

LADON is a long non-coding RNA and natural antisense transcript of the *NODAL* gene, identified by the Collignon team during their investigation of the latter in melanoma progression. In line with findings from other groups, they showed that *NODAL* is not expressed in melanoma. Instead, they discovered that the tumour-promoting activity previously attributed to *NODAL* is mediated by *LADON*. *LADON* expression increases over four days in culture, promoting the mesenchymal-to-amoeboid transition, a process critical to melanoma invasiveness. However, the precise mechanism by which *LADON* exerts its effects remains unclear. Furthermore, previous studies focused on exon 2 deletion, leaving the role of other regions unexplored. To address this, we deleted the full *LADON* locus and observed strong effects on cell proliferation, morphology, and migration, often more pronounced than with exon 2 deletion, suggesting critical roles for exon 2-flanking regions. Proteomic analysis revealed that *LADON* modulates Rho/ROCK and Rac1 pathways, leading to features consistent with amoeboid migration. Additionally, we found that the 3' region of *LADON* might exert a repressive effect on its own transcription. These findings highlight *LADON* as a key player in melanoma progression and the need for deeper investigation into its full-length structure and molecular function.

Introduction

Physio-pathological functions of long non-coding RNAs (lncRNAs)

LncRNAs are a highly heterogeneous group of transcripts that affect gene expression through several mechanisms in both physiological and pathological conditions [1,2]. Mechanistically, lncRNAs can exert their functions both in the nucleus and the cytoplasm (Fig. 1). In the nucleus, they modulate the activity of chromatin remodelling complexes, splicing factors, and transcription factors, and contribute to higher-order nuclear organization by mediating chromatin looping to regulate gene expression. In the cytoplasm, lncRNAs may act as miRNA sponges to prevent mRNA degradation, serve as scaffolds that facilitate protein–protein interactions, or regulate translation rates [1,2]. LncRNAs are vital to genomic imprinting, dosage compensation, pluripotency-regulation and organism development [3]. In the context of skin, lncRNAs are increasingly recognized as key players in development, homeostasis and wound healing [4]. For instance, the lncRNA *TINCR* (Terminal differentiation-induced ncRNA) has a crucial role in the stabilization of mRNAs involved in keratinocyte differentiation [4].

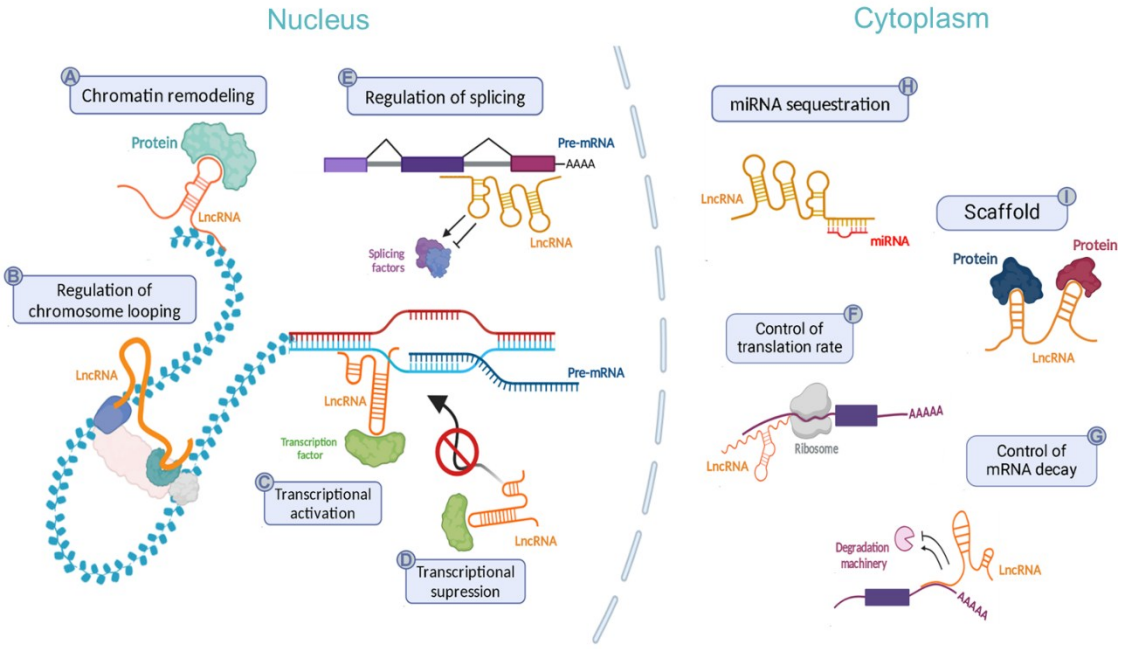

Figure 1. Mechanisms of lncRNA according to the subcellular localization.

LncRNAs (in orange) recruit chromatin-modifying complexes to deposit either activating or repressive histone marks **(A)**, contribute to the spatial organization of the genome by facilitating chromatin looping **(B)** and either guide or sequester transcription factors and core machinery components to specific loci **(C, D)**. They can also modulate pre-mRNA splicing by directly binding to transcripts **(E)**. In the cytoplasm, lncRNAs influence translation by affecting polysome loading **(F)**, regulate mRNA stability by either protecting transcripts or promoting their degradation **(G)**, and serve as molecular sponges for

microRNAs, thereby modulating the expression of miRNA target genes **(H).** Finally, they can also function as scaffolds to regulate protein-protein interactions. Diagram created with Biorender.com and conceptually adapted from *MV Neguembor et al. (2014)*.

However, due to their strong regulatory influence on gene expression at several levels, the expression level of lncRNAs is frequently dysregulated in tumours and, in some cases, they are directly associated with the conversion of normal cells into malignant ones [1]. Indeed, growing evidence suggest lncRNAs as novel biomarkers for diagnosis and prognosis of mis-regulation of cellular processes, which often results in cancer [5], but also as potential targets for therapy or as tools to correct defective gene expression underlying cancer and other pathologies [6].

Uncovering *LADON*

Cancer cells can exploit normally dormant embryonic pathways, such as the TGF-β signalling pathway, to promote tumorigenicity and metastasis. These pathways are based on specific molecules that cancer cells can use to sustain their plastic phenotype. Indeed, understanding the impact of these embryonic signals and the regulatory programs that reactivate them is crucial for the development of new cancer therapies [7].

NODAL, a member of the transforming growth factor β (TGFβ) superfamily, plays a crucial role in mesoderm and endoderm formation, left-right patterning, neurogenesis, and maintenance of stem cell pluripotency [8]. It is also expressed in some adult tissues that undergo periodical renewal or remodelling, such as the endometrium and the mammary gland [9, 10].

Coherently with its physiological function in embryonic and adult tissues, the *NODAL* gene was identified as a possible player in the acquisition of metastatic behaviour in many types of cancer [11]. It was first described in melanoma cell lines as a critical regulator of growth, plasticity, and tumorigenicity, and has since emerged as a promising new biomarker for metastatic potential [11].

However, its actual role in melanoma tumour progression and metastasis was controversial, since *NODAL* expression was not always detected in melanoma [12]. A review of available *NODAL* expression data in cancer cells suggested the existence of distinct splice variants, all including the second exon of the gene [7]. Notably, the predominant transcript in aggressive melanoma cells lacked the third and final exon and thus was incapable of encoding a functional ligand [7]. This evidence was difficult to reconcile with the canonical SMAD2,3-dependent *NODAL* signalling involved in melanoma, since the activation of this pathway would require

the presence of a mature ligand. These findings raised the possibility of a ligand-independent function of the gene in melanoma tumour progression, and they prompted a reassessment of the role attributed to *NODAL* in melanoma.

The Collignon team used both genetic and pharmacological strategies to assess the involvement of *NODAL* in melanoma tumour progression and invasion. In line with the findings of Findlay & Postovit results [1], they found that *NODAL* is not expressed in several metastatic melanoma cell lines and therefore does not contribute to the invasive phenotype. Instead, they identified a long non-coding natural antisense transcript (NAT) that overlaps with *NODAL* exon 2. They named this transcript *LADON*, and showed that it is involved in melanoma tumour progression and metastasis [13].

LADON characteristics and function reported so far

LADON is a 1728nt long RNA (AC022532) transcribed from the plus strand (opposite to *NODAL*) starting from *NODAL* intron 2 and ending in *NODAL* intron 1, and therefore including a sequence complementary to that of the entire *NODAL* exon 2. This NAT contains an open reading frame (ORF) but lacks a canonical Kozak consensus sequence at the start codon (ATG), and no associated protein product has been identified for now. For this reason, it is currently annotated as a non-coding RNA (ENST00000624563.1) [13].

LADON expression has so far been reported in melanoma, breast cancer, colorectal adenocarcinoma, ovarian cancer and lung carcinoma epithelial cell lines [12,14,15], but is likely to be present in other cancer cell lines. There is evidence that it is present in healthy human cell types and tissues, where we currently have no indication of its function.

The Collignon team reported that the deletion of exon 2 drastically reduced the capacity of A375 cells to acquire an invasive phenotype, suggesting a pro-metastatic function of *LADON*. In particular, the expression of this transcript in A375 cells depends on WNT/β catenin signalling and increases 4-fold after 3 days in culture [14]. On the contrary, A375ΔE2 clones, which express a truncated *LADON* transcript consisting of only the 5' and 3' regions flanking exon 2, showed no evidence of increased expression. This suggested that the deletion removed a critical regulatory element necessary for *LADON*'s function. Notably, the increased *LADON* expression was found to promote mesenchymal-to-amoeboid transition, a pivotal mechanism linked to tumour aggressiveness and survival [18,19,20], and to play a role in the regulation of oncogenes and tumour suppressor genes [13].

Finally, a noteworthy feature of *LADON* is the presence of short interspersed nuclear elements (SINEs) Alu and MIR in its 5' and 3' regions. The presence of Alu elements in lncRNAs has been associated with the capacity of such transcripts to regulate RNA transcription, decay or splicing, while the presence of other SINEs has been associated with the regulation of other processes, such as translation [13]. Determining whether these repetitive elements play a role in *LADON's* functions is key to gaining a comprehensive understanding of this transcript.

The mesenchymal to amoeboid transition

Tumour cells can spread to invade other tissues through multiple mechanisms, underlying a high plasticity of cancer cell invasion [16]. These diverse migratory strategies, including collective cancer cell migration and individual types of movement, rely on dynamic changes in cytoskeletal organization and alteration of their contacts with the extracellular matrix and the surrounding stromal cells [19,20].

Recent evidences reported that melanoma cells can interconvert between two main modes of individual movement: a mesenchymal mode characterized by an elongated morphology and an amoeboid mode where cells have a rounded morphology and reach the highest migration efficiency [19,20] (Fig. 2).

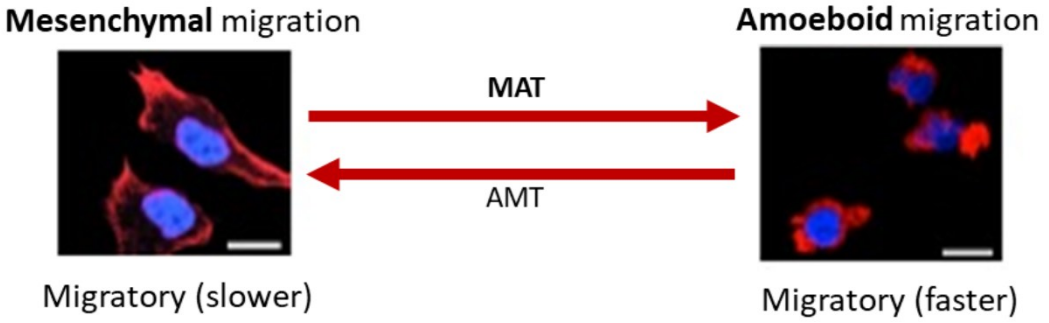

Figure 2. The plasticity in melanoma cell invasion.

Representative images of the A375 cells with elongated or rounded morphology, visualized after F-actin (red) and Hoechst 33342 (nuclear, blue) staining. Scale bar 25µm (*Dutriaux A. et al., 2023*). MAT: Mesenchymal to Amoeboid Transition; AMT: Amoeboid to Mesenchymal Transition.

Mesenchymal cells require cytoskeletal contractility, integrins-mediated ECM-adhesion and proteolysis of the surrounding extracellular matrix [16,18]. Amoeboid cells are characterized by increased migration speed, weak interactions with the extracellular matrix (ECM), and high deformability. A key feature of this migration mode is the elevated actomyosin contractility, which is crucial for enabling these cells to infiltrate through narrow gaps within the ECM [16]. Furthermore, the tension generated by the cortical actomyosin network promotes the formation of membrane blebs, which further contribute to cell motility [16,18,19,20].

Amoeboid and mesenchymal types of migration are mutually interchangeable. The shift towards one type of migration rather than another, notably known as mesenchymal to amoeboid transition (MAT) or amoeboid to mesenchymal transition, is controlled in metastatic A375 melanoma cells by two main signalling pathways: rounded invasion is controlled by Rho/ROCK signalling, whereas elongated movement is prompted by Rac signalling [20]. These transitions

generally rely on the reorganization of the actin cytoskeleton and arise in response to specific cues from the local tumour microenvironment [19,20].

Among these specific signals that could develop during tumour progression an example is represented by energy deprivation. Under conditions of metabolic stress, tumour cells undergo a bioenergetic reprogramming to adapt their energy consumption and in particular to reduce the energy-costly biological processes, for instance by inhibiting the mTOR pathway, which delays RNA translation [21]. Remarkably, the generation of hostile microenvironments due to nutrient deprivation, hypoxia and acidosis induce tumour cells to escape from these perturbated sites, resulting more likely in a mesenchymal to amoeboid transition [21]. Indeed, multiple studies have shown that amoeboid cancer cells exhibit very low energy consumption, mainly due to the reduced energy-demanding interactions with the extracellular matrix and the suppression of both oxidative respiration and glycolysis [21]. These metabolic features make amoeboid migration an effective survival strategy for melanoma and other invasive tumour cells, enabling them to overcome environmental challenges such as nutrient deprivation. As a result, this migration mode is an emerging driver of cancer aggressiveness [19].

Aim of the project

The objective of this project is to contribute to the identification of the regions within *LADON* that are critical for its pro-metastatic function. To this end, I established a phenotypic baseline by characterizing the effects of a complete *LADON* knockout, with the perspective of deleting subregions of interest and studying the resulting mutant phenotypes. As mentioned before, the Collignon team previously characterized the exon 2 mutants.

My project is focused on the study of *LADON* full knockout (KO) mutant cells (A375ΔFL): firstly, I analyzed the effects of the entire removal of *LADON* on cell proliferation, transmigration rate, cell roundness and kinetic of RNA expression, by comparing A375ΔFL clones with A375 cell line and exon 2 mutants (A375ΔE2).

Secondly, I compared the proteomes of the unmodified A375 cell line clones and A375ΔFL to identify a wider range of potential molecular targets of *LADON*, providing insights into the molecular basis of the observed effects in mutant phenotypes. Lastly, to have consistent results, proteomic data must be validated through complementary experiments. To achieve this, as a first step of the validation, I performed RT-qPCR experiments to measure the mRNA expression of selected proteins of interest.

Materials and methods

Cell line, clones and cell culture

The human melanoma A375 cell line was purchased from ATCC. On this cell line, CRISPR/Cas9 genome editing was performed with GeneArt CRISPR Nuclease Vector Kit according to manufacturer's instructions (Life Technology) to generate the following clones:

- Control 1 (Ctrl 1) and control 2 (Ctrl 2*)*: Since the parental cell line A375 is a heterogeneous population of cells, exhibiting aneuploidy and chromosome rearrangements, some of the results may be influenced by this intrinsic heterogeneity. In accordance with this, we generated control A375 cells by treating the parental line with scrambled sgRNA (unmodified A375 cells).
- A375ΔFL22 and A375ΔFL34: full KO of *LADON* clones.
- A375ΔLAD3' a, A375ΔLAD3' b and A375ΔLAD3' c: *LADON* 3'-deleted clones.

Cells were grown in DMEM/F12 Glutamax (Invitrogen, Cergy- Pontoise, France) supplemented with 1% Penicillin-Streptomycin and 10% fetal calf serum (FCS) in a 5% CO2 atmosphere.

Cell growth analysis

A375, A375ΔFL and control cells were seeded at the same concentration in 25cm^2 flasks using 3 ml of DMEM/F12 Glutamax (Invitrogen, Cergy- Pontoise, France) supplemented as described previously. The number of flasks per clone was equal to the number of time points needed for building the cell growth curve (24h, 48h, 72h and 96h). To be counted, melanoma cells were detached incubating them with 0,8 ml of Trypsin-EDTA (0.05%) phenol red (Thermo Fisher Scientific, Waltham, Massachusetts, USA) for 1.5 min at 37°C. Trypsin was inhibited through the addition of 3ml of medium supplemented with 10% fetal calf serum (FCS). 10 µl suspension of detached melanoma cells were mixed with 10 µl of trypan blue solution and subsequently loaded into a Countess™ Cell Counting Chamber Slide (Invitrogen™, Thermo Fisher Scientific, USA). The measure of the number of cells/ml was performed through Countess™ 3 FL Automated Cell Counter (Invitrogen™, Thermo Fisher Scientific, USA).

Transmigration assay

Transmigration assay allow us to test the invasive properties of tumour cells *in vitro*. Melanoma cells (4×10^5) were seeded on the upper compartments of 2 mg/ml type I collagen-coated culture inserts (8 µm pores-Greiner Bio-One SAS, Courtaboeuf, France). This collagen matrix layer serves as a barrier to discriminate invasive cells

from non-invasive cells. Invasive cells are able to degrade the collagen matrix layer and ultimately pass through the pores of the polycarbonate membrane. DMEM supplemented with 10% FCS was used as a chemoattractant. A375, controls and ΔFL mutant cells were allowed to migrate at 37°C and 5% CO2 for 24h. Non-migrating cells on the upper face of the filter were removed by gently scraping them off using a cotton swab. Cells on the lower face were washed in PBS, fixed with 4% formaldehyde and washed in PBS. Nuclei were then labeled with Hoechst and washed again. Afterwards, the filter was cut and softly placed onto a drop of mounting medium (Fluoromount G, Invitrogen) on a microscope slide, then sealed. Migrating cells on the lower part of the filter were counted under an epifluorescence microscope using a 20x magnification. The counting procedure has been performed in at least 20 adjacent fields of each Transwell. P-values were calculated by two-sided student's t-test.

Roundness analysis

A375, A375ΔFL and control cells were grown in 25cm^2 flasks using DMEM/F12 Glutamax (Invitrogen, Cergy- Pontoise, France) supplemented as described previously. Five to ten pictures of different fields of each clone's flask were taken at several time points (24h, 48h and 72h of culture). Roundness was calculated through the following formula: $R = 4\pi * \frac{A}{L^2}$ for 20 different cells among the several images of a specific clone, by using the IMAGEJ software (US National Institutes of Health, Bethesda, MD, USA). All the measures were summarized in a histogram graph and P-values were calculated by two-sided student's t-test.

RNA extraction and reverse transcription (RT)

Total RNA extraction was performed starting from cells cultivated as previously described using NucleoSpin RNA isolation kit (Macherey-Nagel, Duren, Germany) following producer's instruction.

The retrotranscription was performed on 300ng of total RNA using SuperScript VILO cDNA Synthesis kit (Thermo Fisher Scientific, Waltham, Massachusetts, USA) following producer's instruction.

PCR and Quantitative PCR (qPCR)

PCR and qPCR were performed using, respectively, REDTaq ReadyMix PCR Reaction Mix (Sigma-Aldrich, Saint-Louis, Missouri, USA) and LightCycler FastStart DNA Master SYBR Green I (Roche, Bâle, Suisse) following producer's instructions. When performing qPCR, for each gene and for a given RT sample, values were normalized to the level of expression of housekeeping gene GADPH or RPL13. For each RT sample, RNA expression level was measured in duplicate.

Sequence and annealing temperatures for all primers used were designed using Primer Blast tool (https://www.ncbi.nlm.nih.gov/tools/primer-blast/):

Primers used for PCR and RT-qPCR				
Name	**Localization**	**Sequence**	**Product length**	**T annealing (°C)**
A3	Chr 10 pos. 70434204	GGCAGGGCCACCTATAACAT	558	59
F6	Chr 10 pos. 70437046	TGGGTTTGGTTGTCTTGGGT	89	59.7
L2F	Chr 10 pos. 70435161	TGGTACATTGGAGGTGCTTG	188	60
L2R	Chr 10 pos. 70435349	TGAGGGCGAGTGTCCTAATC		
ITGB4 F	Chr 17 pos. 75752174	TCAACGATGACAACCGACCT	73	59
ITGB4 R	Chr 17 pos. 75752231	AGCAGCATCCGGTTCTTAGG		60
ARHGAP29 F	Chr 1 pos. 94177654	CGCAAGCAAAATGCGTTAGGA	60	60
ARHGAP29 R	Chr 1 pos. 94177612	AAGCAACTGTGCTTTGTCACTG		60
ARHGDIB F	Chr 12 pos. 14949888	ACCCTGGTTTGTGAGAGTGC	65	60
ARHGDIB R	Chr 12 pos. 14949829	AGGGCTTCCAGATCTCCAGTA		59
DOCK2 F	Chr 5 pos. 169714359	AGCTCACTCAGAATGTGGGC	68	60
DOCK2 R	Chr 5 pos. 169714412	CTCCTGTAGCAGTTGAGGCT		59

CRISPR/Cas9 genome editing

CRISPR/Cas9 genome editing was performed with GeneArt CRISPR Nuclease Vector Kit (Life Technologies, Carlsbad, California, USA) following producer's instructions.

A375ΔFL clones were generated using following oligos:

CRISPR 5' *LADON*FL Top	**F-**	**GAACAGTGTGATTCCAACCG**
CRISPR 5' *LADON*FL Bottom	**R-**	**CGGTTGGAATCACACTGTTC**
CRISPR 3' *LADON*FL Top	**F-**	**CCAGGTCATTCACACACCTG**
CRISPR 3' *LADON*FL Bottom	**R-**	**CAGGTGTGTGAATGACCTGG**

A375ΔLAD3' clones were generated using following oligos:

CRISPR 5' Exon 2 deletion Top	**F-**	**ATCCACTGCCACATCTGGGT**
CRISPR 5' Exon 2 deletion Bottom	**R-**	**ACCCAGATGTGGCAGTGGAT**
CRISPR 3' *LADON*FL Top	**F-**	**CCAGGTCATTCACACACCTG**
CRISPR 3' *LADON*FL Bottom	**R-**	**CAGGTGTGTGAATGACCTGG**

The abovementioned ds oligonucleotides were cloned into the GeneArt CRISPR Nuclease Vector. Competent E. Coli cells were transfected with 4,5 µL of ligation reaction and then 100 µL from the transformation reaction were spread on a pre-warmed LB agar plate containing 100 µg/mL ampicillin.

Plates were incubated overnight at 37°C. The next day minipreps were prepared picking some colonies and putting them to grow overnight in 3 ml of LB containing 50 µg/mL ampicillin in an incubator at 37°C and 200rpm shake. The next day the plasmidic DNA was purified with NucleoSpin Plasmid miniprep kit (Macherey-Nagel, Duren, Germany) following producer's instructions, and then the identity of the ds oligonucleotide insert in positive transformants was

confirmed by sequencing the plasmids with U6 primer, as indicated in the GeneArt CRISPR Nuclease Vector Kit.

Cells were then transfected with the clones containing the correct insert using Lipofectamine 2000 Reagent (Life Technologies, Carlsbad, California, USA): for each 25 cm2 flask seeded with 2,5 million A375 cells in 3 ml of medium without antibiotics 20 µL of lipofectamine and 4 µg total of plasmidic DNA (2 µg of each plasmid) were used.

After 72h, cells highly transfected were sorted by FACS thanks to OFP, a fluorescent protein present in the GeneArt CRISPR Nuclease Vector. To prepare the cells for sorting they were detached using trypsin, then centrifuged and suspended in PBS 1X containing 1 mM EDTA and 1% FCS to reach a concentration of 3 million cells/ml, and lastly filtered with an appropriate sterile filter.

A control composed by cells treated with sole lipofectamine was used as a comparison to select the most fluorescent cells, that were recovered in a 96 wells plate where single cells were seeded in 150µl of DMEM/F12 glutamax supplemented with 1% Penicillin-Streptomycin and 20% FCS. A backup sample of 3000 cells was recovered in a 1,5 ml Eppendorf filled with 1ml of DMEM/F12 glutamax supplemented with 1% Penicillin-Streptomycin and 20% FCS and then seeded in 10 ml of DMEM/F12 glutamax supplemented with 1% Penicillin-Streptomycin and 15% FCS in a 10cm plate.

To test if the deletion occurred successfully, a PCR was performed using some primers mapping upstream or downstream the deletion site.

Protein extraction and quantification

Control 1, control 2, A375ΔFL22 and A375ΔFL34 cells were grown in 25cm^2 flasks to extract proteins after 24h, 48h and 72h of culture. To perform protein extraction, melanoma cells were detached as previously described, centrifuged at 900 rpm for 3.5 minutes, rinsed with 1 mL of 1X PBS, and centrifuged again. Each cell pellet was then resuspended with 180 µl of cold TP RIPA buffer, 10 µl of protease inhibitor (stock 20X, Roche) and 10 µl of phosphatase inhibitor (stock 20X, Roche). Bioruptor® Sonicator (Diagenode, Liège, Belgium) in cold room (4 °C) was used to disrupt cells (interval: 0.5; force H: max; time: 10 minutes). Finally, each cell lysate was centrifugated for 15 min at 12000 rpm at 4 °C. Proteins in supernatant were stored at – 80 °C. Protein extraction was performed in duplicate.

Protein quantification was performed through spectrophotometer. Standard curve was generated by using BSA (stock 10 mg/ml) as standard protein. Dye-based protein detection was either performed using BRADFORD assay (Thermo Fisher Scientific, Waltham, Massachusetts, USA), or using BCA assay (Thermo Fisher Scientific, Waltham, Massachusetts, USA).

Samples preparation prior to LC-MS/MS analysis

A six-time volume of cold acetone (−20°C) was added to a sample volume containing about 10 µg of protein extracts. Vortexed tubes were incubated overnight at -20°C then centrifuged for 10 min at 11000 rpm, 4°C. Supernatant was removed, then the protein pellets were dissolved in urea 8M - NH4HCO3 25mM buffer. Samples were then reduced with TCEP-HCl 10 mM and alkylated with MMTS 20 mM. After a 16-fold dilution in NH4HCO3, samples were then digested overnight at 37°C by a mixture of trypsin/Lys C (1/100 Enzyme/Substrate ratio). Before LC-MS/MS analysis, the digested peptides were loaded and desalted on evotips provided by Evosep (Odense, Denmark) according to manufacturer's procedure.

LC-MS/MS acquisition

Samples were analyzed on a timsTOF Pro 2 mass spectrometer (Bruker Daltonics, Bremen, Germany) coupled to an Evosep one system (Evosep, Odense, Denmark) operating with the 40SPD Whisper Zoom method developed by the manufacturer. Briefly, the method is based on a 32-min gradient and a total cycle time of 38 min with a C18 analytical column (0.075 x 150 mm, 1.7µm beads, ref Aurora Elite CSI from IonOpticks) equilibrated at 50°C and operated at a flow rate of 200 nL/min. H2O/0.1 % FA was used as solvent A and ACN/ 0.1 % FA as solvent B. The timsTOF Pro 2 was operated with a DIA-PASEF method comprising 12 pydiAID frames with 3 mass windows per frame resulting in a cycle time of 0.975 seconds as described in Bruker application note LCMS 218. Collisional energy was ramped stepwise as a function of ion mobility.

Material used for LC-MS/MS analysis

MS grade Acetonitrile (ACN), H2O and formic acid (FA) were from ThermoFisher Scientific (Waltham, MA, USA). Sequencing-grade trypsin/Lys C mix was from Promega (Madison, WI, USA). Ammonium bicarbonate (NH4HCO3) was from Sigma-Aldrich (Saint-Louis, MO, USA).

Data analysis

MS raw files were processed using Spectronaut version 19.4.241104.62635. Data were searched against the SwissProt Homo Sapiens database (downloaded January 2025, 20649 entries). Parent mass tolerance was set to 20 ppm, with fragment mass tolerance at 0.05 Da. Specific tryptic cleavage was selected and a maximum of 2 missed cleavages was authorized. For identification, the following post-translational modifications were included: Acetyl (Protein N-term), Oxidation (M), and Deamidation (NQ) as variables and betamethylthiolation (C) as fixed. Identifications were filtered based on a 1% Q-value threshold at both precursor and protein levels. Quantification was performed using Spectronaut Quantification

Module, with all default parameters. Proteins were inferred using the automatic features of Spectronaut, with the algorithm IDPicker.

Multivariate statistics on protein or peptide measurements were performed using Qlucore Omics Explorer 3.9 (Qlucore AB, Lund, SWEDEN). A positive threshold value of 1 was specified to enable a log2 transformation of abundance data for normalization i.e. all abundance data values below the threshold will be replaced by 1 before transformation. The transformed data were finally used for statistical analysis i.e. evaluation of differentially present proteins or peptides between two groups using a Student's bilateral t-test. A p-value better than 0.01 was used to filter differential candidates.

Proteomic analysis

Differentially expressed proteins were analyzed using ShinyGO v0.82 (South Dakota State University, Brookings, SD, USA), Metascape (Johns Hopkins University, Baltimore, MD, USA), NDEx v2.5.8 (University of California San Diego, La Jolla, CA, USA) and RStudio (Posit Software, PBC, Boston, MA, USA).

Statistical analysis

Data was collected and graphed using GraphPad Prism software. A 1-way ANOVA or two-sided student's t-test was used to determine statistical significance where appropriate. P-values of less than 0.05 were considered statistically significant. Additional information about the statistics used for each experiment can be found in the relevant figures or figure legends.

Results

LADON expression affects the proliferative potential of A375 melanoma cells

To investigate the role of *LADON* in a more holistic manner, we used genome editing to delete the entire sequence of this non-coding gene (Fig. 3A). This allowed us to obtain several independent full-length knockout (FL KO) mutant clones, designated as A375ΔFL. We focused on two of these clones, A375ΔFL22 and A375ΔFL34, and characterized them using PCR (Fig. 3B).

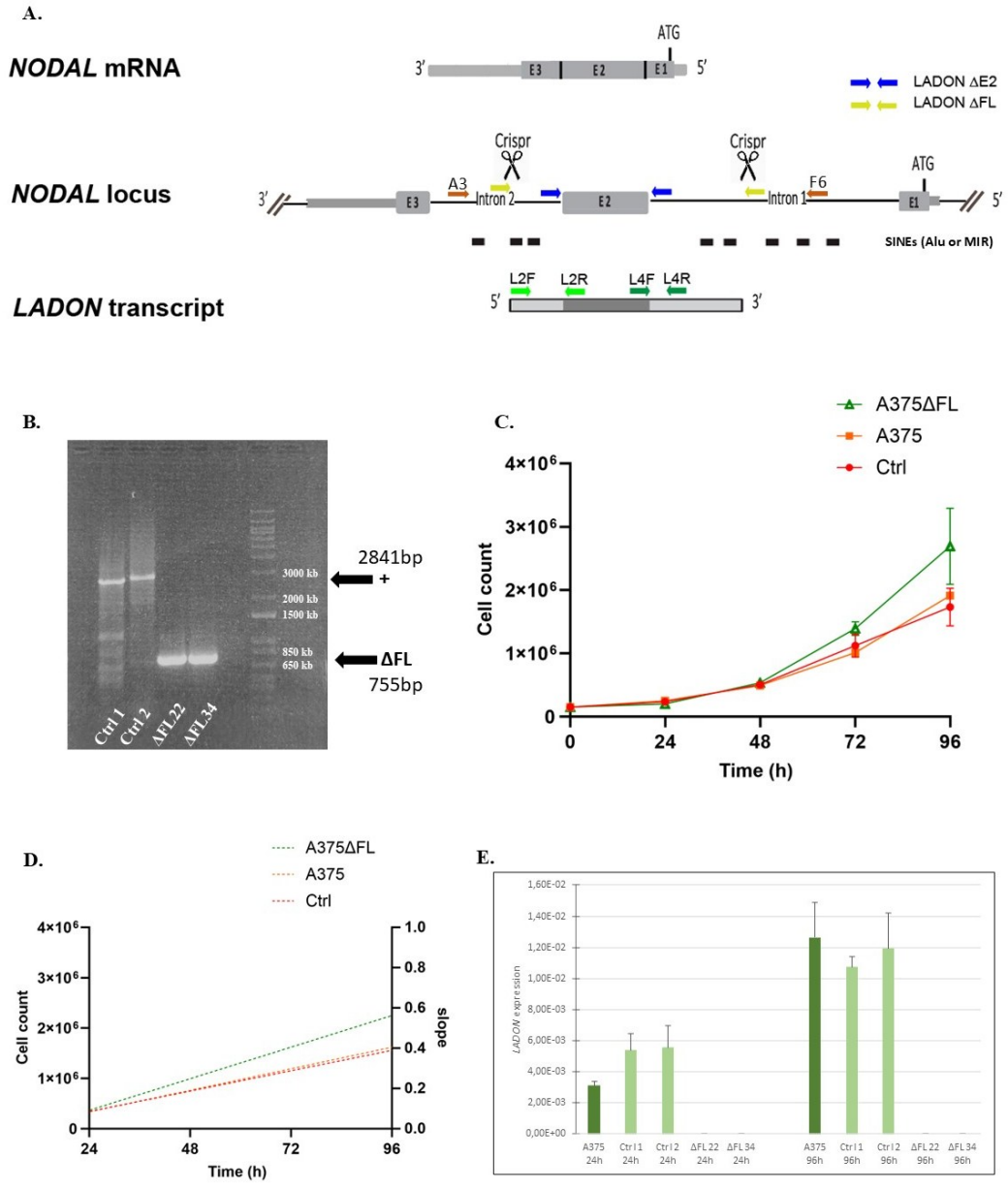

Figure 3. *LADON* deletion and its involvement in cell proliferation.

(**A**) Schematic of the human *NODAL* locus with its 3 exons (E1 to E3), showing the full-length *NODAL* mRNA above, and the *LADON* transcript transcribed from the opposite strand below. The complete deletion of *LADON* transcript led to the generation of A375ΔFL mutants. A3 and F6 primers were used to identify the mutants through PCR. The

arrows in green represent the primers used to track *LADON* transcript. The black boxes show the location of short interspersed nuclear elements (SINEs), which are mostly Alu and MIR sequences. (**B**) PCR analysis of DNA extracted from unmodified A375 cells (Ctrl 1 and Ctrl 2) and mutant cells (A375ΔFL22 and A375ΔFL34) using A3 and F6 primers. Considering CRISPR Cas9's conditions, we were expecting a band of 2841 kb for Ctrl cells and a band of 755 kb for mutants where deletion occurred. + and ΔFL indicate unmodified and *LADON* full length-deleted clones respectively. (**C**) In vitro-generated growth kinetic curve, across 4-days culture, for parental cell line A375, unmodified A375 clones and A375ΔFL. For each time point, Ctrl and mutant cell count values were averaged over two independent measurements. (**D**) A simple linear regression analysis was performed using GraphPad Prism to determine the slopes of the best-fit lines corresponding to the growth curves shown in panel (C). The slope coefficient represents the rate of change in cell growth over time, providing a quantitative measure of proliferation dynamics. (**E**) RT-PCR with primers (L2F and L2R) amplifying a region of 188 nt specific to *LADON* detecting an increase of *LADON* expression between 24h and 96h of culture in A375 and control cells. As expected, no amplification was observed in A375ΔFL clones, confirming the absence of *LADON* expression in these mutants. Moreover, for each time point, the expression levels of *LADON* in the controls (Ctrl 1 and Ctrl 2) were comparable to those in the parental A375 cells, with no significant differences observed. The histogram display mean values ± SD.

Previous data had shown that *LADON* knockdown (KD) cells reached confluence more rapidly than control cells [13]. To assess *LADON*'s involvement in regulating proliferation, cell growth experiments were conducted to compare the proliferative capacity of parental A375 cells with that of *LADON* full knockout (KO) mutants. Growth curves were generated, showing that A375ΔFL cells have higher proliferation rates compared to their parental line, after 48h of culture (Fig. 3C). This observation was further supported by calculating the slope of each growth curve using a simple regression model, where we can notice steeper slopes for A375ΔFL growth curves compared to controls (Fig. 3D).

These results suggest that *LADON* negatively impacts the proliferation rate of A375 melanoma cells. Some evidence showed that melanoma cells can be defined by either a proliferative or invasive transcription signature: two distinct and interconvertible states that cannot co-exist within the same cell [22]. Consistently with this, the absence of *LADON* potentially forced A375ΔFL cells to maintain a more proliferative and non-invasive cell identity compared to the controls in which *LADON* expression is induced.

A noteworthy observation is that the difference in proliferation rates between A375ΔFL cells and control cells becomes significant only after 48 hours of culture. This is likely due to the presence of a lag phase preceding exponential growth, during which cells adapt to the culture conditions. Furthermore, in metastatic melanoma cells *LADON* expression significantly increases between 24h and 96h of culture (Fig. 3E), leading presumably to a delayed effect on proliferation rate. This

suggests a concentration-dependent influence of *LADON* on proliferation and/or that its effects are mediated through downstream regulatory mechanisms that require time to manifest.

LADON promotes invasion likely through mesenchymal to amoeboid transition

Melanoma cells appear to be highly plastic and can convert between two main different modes of movement: mesenchymal and amoeboid. Among these, the amoeboid mode, characterized by its greater speed, is reported to be the most efficient strategy for promoting invasive behaviour [19]. We therefore investigated the effect of the complete deletion of *LADON* on migrating behaviour and cell morphology.

Previous results suggested that the expression of a truncated *LADON* transcript, generated after CRISPR deletion of exon 2, notably decreased the transmigration rate when compared to that of the parental line [13]. Indeed, firstly, A375ΔE2 mutants were tested in a transmigration assay to confirm their loss of capacity to migrate to the lower chamber of transwell insert (Fig. 4A). Secondly, to obtain a more comprehensive understanding of *LADON*'s role in inducing invasive features in A375 melanoma cells, we used the transwell transmigration assay to quantify the capacity of seeded A375ΔFL cells to migrate through a collagen layer. We found, as expected, that more A375 cells (mean=7 cells per field) migrated significantly ($P < 0.01$) toward the lower chamber than A375ΔFL cells (Fig. 4A), showing that the absence of *LADON* drastically reduced the cell motility of melanoma cells *in vitro*. The same behaviour is observed for unmodified A375 cells (Ctrl 1 and Ctrl 2), supporting the significance of these results (Fig. 4B). Remarkably, the histogram in Fig. 4A shows that there are no significant differences in the average number of migrating A375ΔFL and A375ΔE2 cells. This suggests that the deletion of exon 2 is sufficient to drastically reduce the capacity of these cells to migrate.

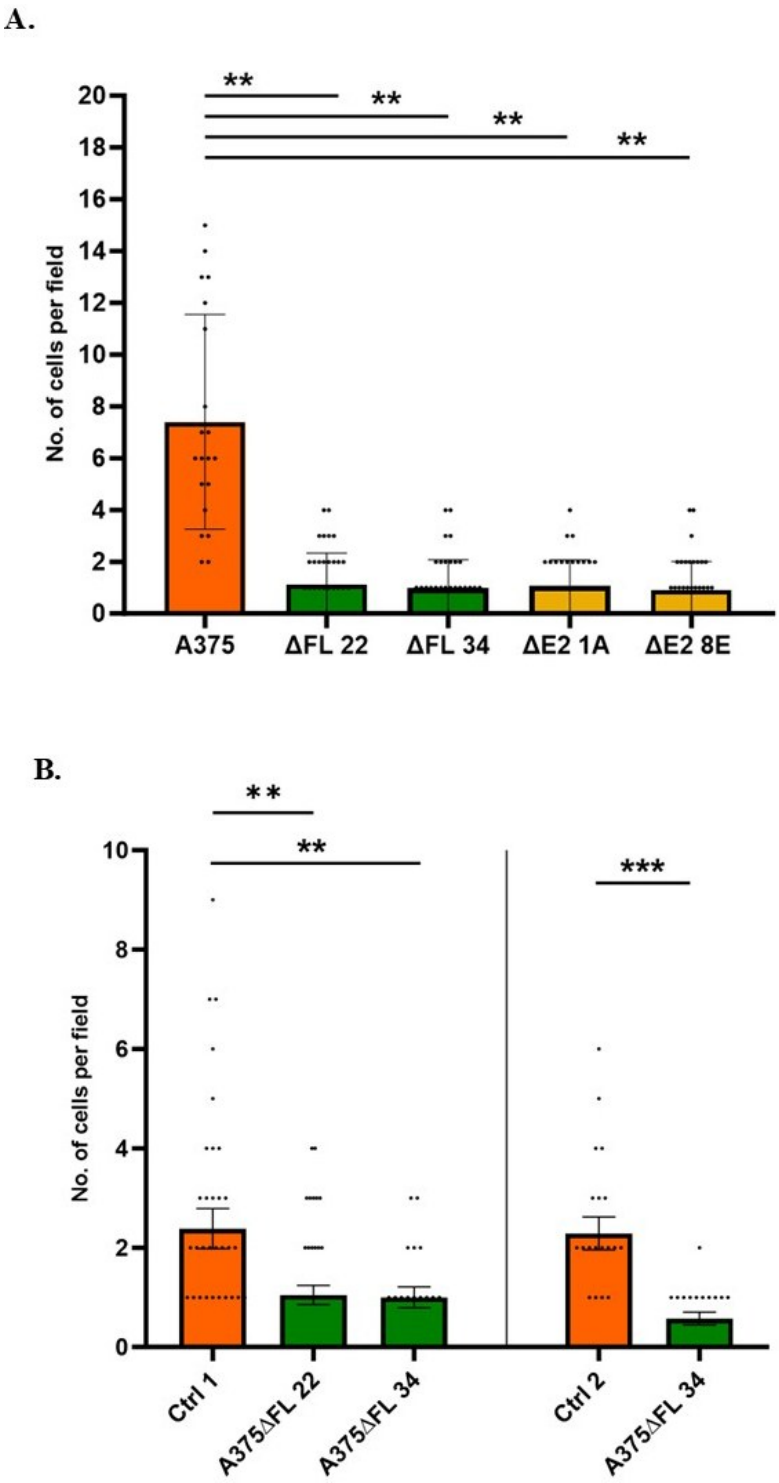

Figure 4. *LADON* involvement in cell motility.

(**A**) Histogram of transmigration assay of A375, A375ΔFL and A375ΔE2 cells. For each transwell slide, at least 20 adjacent fields were considered to count the number of migrating cells. (**B**) Histograms of transmigration assay of unmodified A375 cells (controls) and A375ΔFL cells. The black line divides two independent experiments. Histograms display mean values ± SD. P-values were calculated in a Student's t test, * < 0.05, ** < 0.01, *** < 0.001.

The mesenchymal to amoeboid transition (MAT) involves a change from an elongated to a smaller and rounded cell morphology. Roundness index measurements revealed that the most pronounced differences in cell morphology between A375 and A375ΔFL cells emerged at 48 hours of culture (Fig. 5B). In particular, our results showed that, at this time point, A375 and control cells are significantly ($P<0.01$) more rounded than A375ΔFL cells, which instead are characterized by a more elongated shape (Fig. 5B, 5D), suggesting a time-localized regulatory effect of *LADON* on cell morphology. This effect is not evident at 24h (Fig. 5A), but it's more visible at 72h (Fig. 5C), even if it’s not as pronounced as the one occurring at 48h of culture (Fig. 5B).

These findings imply that *LADON* is involved in maintaining a rounded morphology in A375 cells and may contribute to amoeboid features which are associated with enhanced metastatic potential. Furthermore, since morphological differences between FL mutants and parental cell line become evident at 48h, this time point appears to be crucial, and this suggests a time-dependent influence of *LADON* on cell morphology, cytoskeleton dynamics and migrating behaviour, potentially due to the action of key downstream effectors.

Notably, at both 48h and 72h, the roundness index of A375ΔE2 cells is comparable to that of A375 and control cells (Fig. 5B, 5C), indicating that only the complete knockout of *LADON* significantly impacts cell morphology and the transition between amoeboid and mesenchymal migration modes in melanoma cells.

Another relevant aspect is that, even if A375ΔE2 clones display an amoeboid morphology similar to that of A375 cells, their transmigration rate is markedly reduced, resembling that of A375ΔFL cells (Fig. 4A).

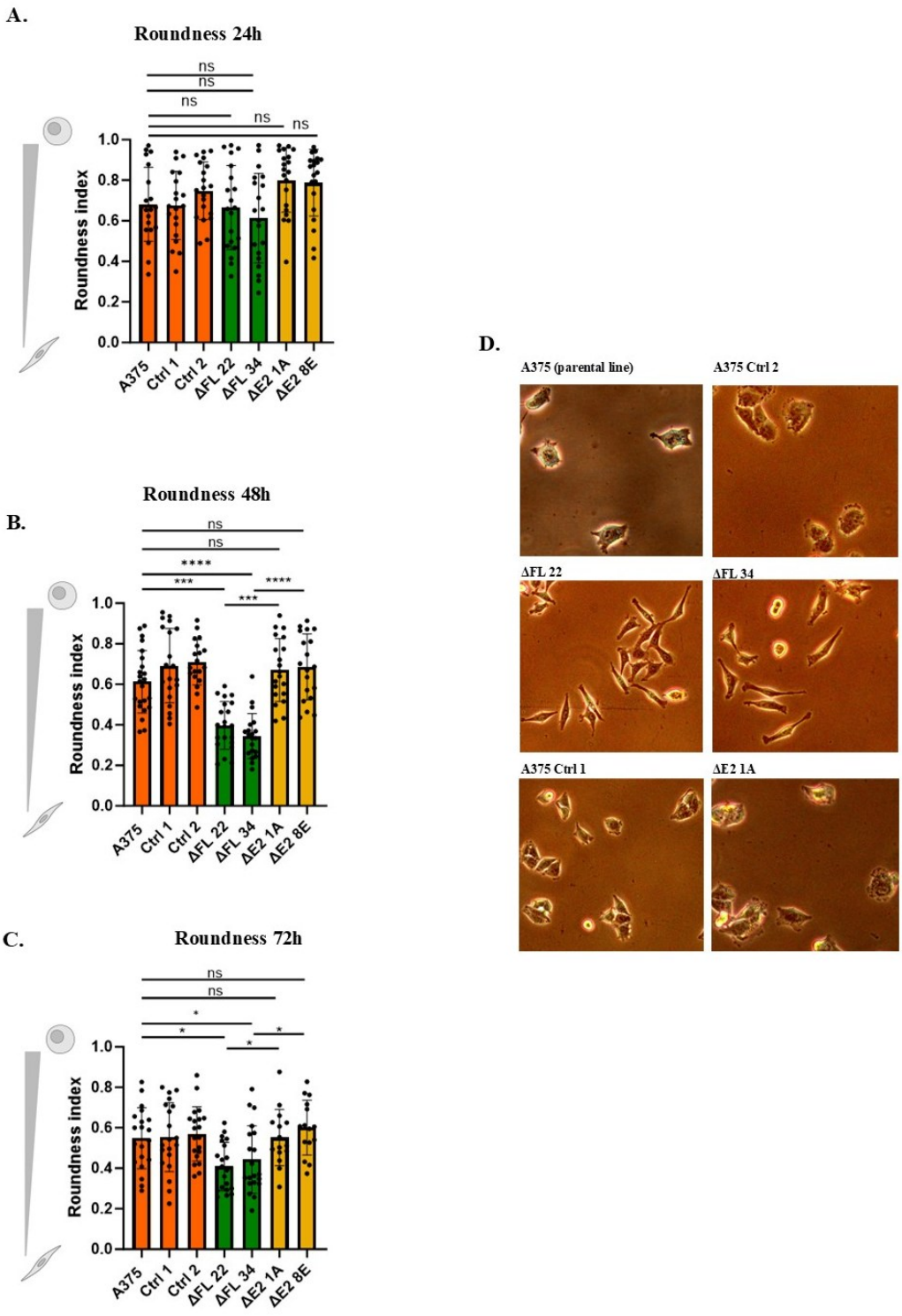

Figure 5. *LADON* involvement in cell morphology.

Histograms show roundness index measurements of A375, Ctrl, A375ΔFL and A375ΔE2 cells cultured for 24h (**A**), 48h (**B**) and 72h (**C**). Roundness was calculated through the following formula: $R = 4\pi * \frac{A}{L^2}$. (**D**) Representative images of A375 cells, unmodified A375 clones (Ctrl 1, Ctrl 2) and mutant cells (A375ΔFL 22, A375ΔFL 34 and A375ΔE2

1A) with elongated or rounded morphology. Images are taken at 20X of magnification after 48h of culture. Scale bar 10 μm.

Histograms display mean values ± SD. P-values were calculated in a Student's t test, * < 0.05, ** < 0.01, *** < 0.001, **** < 0.0001

LADON deletion alters the proteomic landscape in melanoma cells

To identify a wider range of molecular factors acting downstream of *LADON*, we used mass spectrometry to compare the proteomes of control A375 cells and A375ΔFL cells after 24, 48, and 72h in culture. Fold changes were calculated using as reference group the A375ΔFL cells (A375 cells vs A375ΔFL cells), so a negative Log_2 Fold Change (Fold Change inferior to 1) indicates a downregulation tendency of that specific protein within unmodified A375 cells, whereas a positive Log_2 Fold Change (Fold Change superior to 1) reflects a relative overexpression of the protein in these cells.

To have a general view of the data at each time point, we graphed the results in volcano plots representing the comparative analysis for 24h, 48h and 72h (Fig. 6A, 6B, 6C). At 24h and 48h the number of up-regulated proteins (fold change superior to 1.5) is slightly higher (around 25% more) than that of the down-regulated proteins (fold change inferior to 0.66667). However, by 72 hours, no significant difference is observed between the quantity of up- and downregulated proteins, although the total number of significantly dysregulated proteins (404) is the highest of the three time points. These findings suggest that *LADON* may exert an early slightly predominant activating effect at the protein level, which appears to stabilize over time. Therefore, it is not possible to infer a consistent or unidirectional regulatory role for *LADON* based solely on these data.

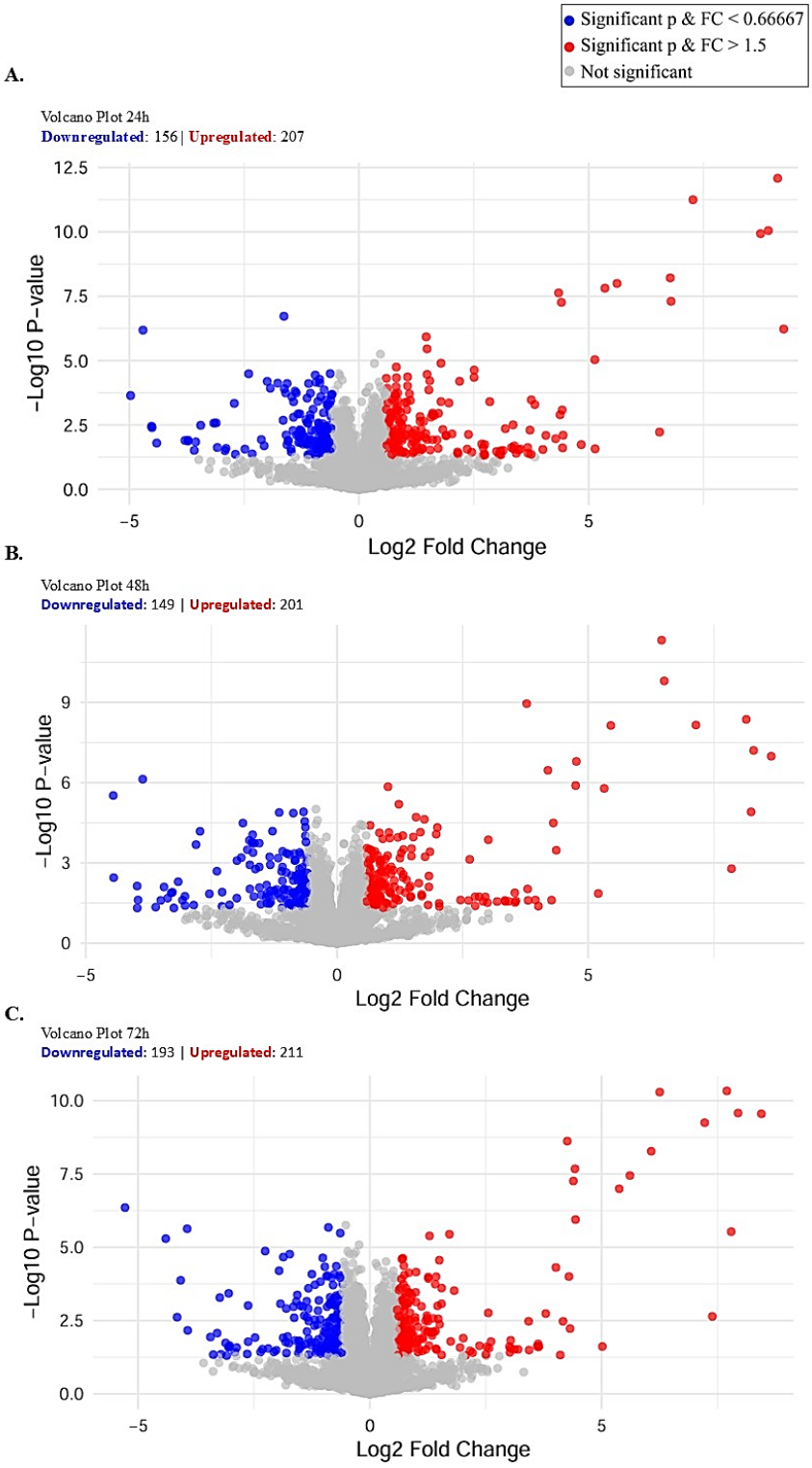

Figure 6. Data visualization (control A375 vs A375ΔFL)

Volcano plot representation of comparative proteomics analysis between unmodified A375 and A375ΔFL cells cultured for 24h (**A**), 48h (**B**) and 72h (**C**). Grey dots: non-significant p-value. Blue dots (downregulated), significant p-value and fold change <0.66667. Red dots (upregulated): significant p-value and fold change >1.5. Fold change values refer to A375 vs A375ΔFL cells. Volcano plots were generated using Rstudio.

LADON affects the level of proteins involved in cytoskeleton organization, ECM-cell interactions and MAT

Results in Fig. 5B suggest 48h is a crucial time point for change in cell morphology. Therefore, we focused on proteins that were identified at 48h by at least 3 independent peptides and with a significant ($P<0.05$) fold change inferior to 0.66667. KEGG pathways analysis showed a significant enrichment in proteins involved in ECM-cell interactions (Fig. 7A), notably integrins (ITGA6, ITGB4, ITGB7), and in focal adhesion (LAMA5, CAV1, CAV2). Furthermore, a Gene Ontology (GO) analysis for biological processes highlighted the enrichment of proteins associated with amoeboidal-type cell migration (Fig. 7B), which is consistent with the results shown in Fig. 5B. Among these 17 proteins, as shown in Table 1, several are implicated in actin cytoskeleton remodelling (PDLIM1, TNS1, DOCK2, FMNL1), while others function as cell surface receptors, including receptor tyrosine kinases (EGFR, MET) and non-kinase receptors (NRP1). Integrins also appeared to be enriched once again in this GO category, underscoring their central role in cell morphology regulation. Interestingly, measuring it through RT-qPCR, ITGB4 RNA in control A375 cells is significantly lower than the one in A375ΔFL cells (Fig. 7C). Finally, most of aforementioned proteins were found to be involved also in regulation of cell migration and cell motility (Fig. 7B).

The expression of all these proteins is down-regulated at 48h in control A375 cells, suggesting that *LADON* plays a repressive role in their expression. Furthermore, the GO term: “amoeboidal-type cell migration” is significantly overrepresented exclusively at the 48-hour time point.

Taken together, these results strongly indicate that *LADON* plays a crucial role in the dynamic organization of the cytoskeleton, which is central to cell morphology changes and migration. Moreover, this transcript may be involved in maintaining a low level of integrins, an effect that is coherent with amoeboid movement, where cancer cells pass through the ECM without relying on integrin-mediated ECM adhesion, which instead is crucial for mesenchymal movement [16]. This could be a reason why at 48h, in the absence of *LADON*, which results in a 7- to 9-fold increase in the expression of integrins, A375ΔFL cells appear more elongated compared to control cells (Fig. 5D).

Protein	Fold Changes A375 Ctrl vs A375ΔFL (48h)	(p) t-test (48h)	ECM-receptor interaction	Ameboidal-type cell migration	Cell motility	Actin cytoskeleton	Accession
Integrin beta-4 (ITGB4)	0,142942394	0,000207068	✓	✓		✓	P16144
Integrin beta-7 (ITGB7)	0,151131489	6,58E-05	✓	✓		✓	P26010
Formin-like protein 1 (FMNL1)	0,341625369	0,000183391				✓	O95466
Laminin subunit alpha-5 (LAMA5)	0,250430416	6,43E-05		✓		✓	O15230
PDZ and LIM domain protein 1 (PDLIM1)	0,410590635	6,51E-05		✓	✓	✓	O00151
Epidermal growth factor receptor (EGFR)	0,443946641	0,000660198		✓	✓		P00533
Neuropilin-1 (NRP1)	0,558032679	0,000818426		✓	✓		O14786

Table 1. Some examples of proteins significantly enriched in KEGG pathways and GO biological processes at 48h.

Finally, receptor tyrosine kinase signalling has been linked to Rac-dependent elongated movement [20]. Among proteins significantly downregulated at 48h, 7 were annotated to be transmembrane proteins with tyrosine kinase activity, whose reduced levels in unmodified A375 cells may help explain the adoption of a more rounded morphology rather than an elongated one.

LADON affects the expression of components of Rho/ROCK and Rac signalling

The plasticity of individual melanoma cell invasion is based on the capacity of these cells to interconvert between a rounded shape and a more elongated one. This high plasticity allows melanoma cells to switch between two different migration modes, which are regulated respectively by Rho/ROCK and Rac signalling [19,20]. Some factors, which are reported to have a role in these two signalling pathways, are found to be dysregulated when comparing unmodified A375 cells to A375ΔFL cells.

Among the downregulated proteins in control cells (fold change inferior to 0.66667), we found Microphthalmia-associated transcription factor (MITF) and Rho GDP-dissociation inhibitor 2 (ARHGDIB) to be significantly repressed in the presence of *LADON*, only at 24h. MITF is reported to be the master regulator of melanoma cell biology and, even if its role in cancer invasion is still under observation, some evidences demonstrated that low levels of this protein are associated with a reorganization of actin cytoskeleton, which results in an increased ROCK-dependent invasiveness (associated to amoeboid movement) [20]. ARHGDIB regulates the GDP/GTP exchange reaction of the Rho proteins by inhibiting the dissociation of GDP from them, and the subsequent binding of GTP to them, suggesting an inhibitory role of this protein towards the Rho/ROCK-mediated amoeboid movement. Interestingly, MITF and ARHGDIB are

significantly repressed only at 24h, indicating that these proteins may be early targets of *LADON*.

Focusing on other players of these signalling pathways, we found ARHGAP29, ARHGAP18, DOCK2 and EPHA3 to be significantly dysregulated at protein level. A 2- to 3- fold increase in the expression of ARHGAP29 and ARHGAP18 proteins in A375ΔFL cells over time (24h, 48h and 72h) is observed, suggesting a repressive role of *LADON* on their expression. These two are Rho GTPase-activating proteins that act by inhibiting Rho GTPases proteins converting them to an inactive GDP-bound state. Similarly, DOCK2 presents a 3-fold increase in its expression in the absence of *LADON* (24h and 48h). This protein is involved in cytoskeletal rearrangements and in the preferential activation of RAC1 and RAC2. Finally, EPHA3 is overexpressed in unmodified A375 cells, showing a 2- to 3-fold increase compared to A375ΔFL cells, supporting a potential activating role of *LADON* in EPHA3 expression. EPHA3, a member of the Eph receptor tyrosine kinase family, has been reported to be involved in retraction of cell protrusions, cell rounding, membrane blebbing and de-adhesion through the transient activation of RhoA [23]. Remarkably, when focusing on proteins that were significantly dysregulated ($P < 0.05$) but exhibited only modest changes in expression ($0.49 <$ fold change < 1.49) we identified additional Rho GTPase-activating proteins associated with the inhibition of Rho/ROCK signalling, such as ARHGAP1 and ARHGAP17, which showed a 1.2- to 1.35-fold increase in expression in A375ΔFL cells. Conversely, proteins known to negatively regulate the Rac1 signalling pathway, including ARFGAP1 and ARHGAP5, displayed a 1.2-fold increase in expression in unmodified A375 cells.

RT-qPCR experiments were conducted to evaluate the RNA expression of some abovementioned factors involved in Rho/ROCK signalling after 24h of culture (Fig.7D, 7E, 7F). Remarkably, both ARHGAP29 and ARHGDIB were found to be significantly downregulated also at RNA level in unmodified A375 cells compared to A375ΔFL cells, suggesting that *LADON*'s regulation for ARHGAP29 and ARHGDIB occurs at transcriptional level, presumably within the nucleus. In contrast, DOCK 2 turned out to be downregulated by *LADON* only at protein level, with no significant difference in RNA expression between control and mutant cells. This suggests the involvement of an alternative post-transcriptional regulatory mechanism.

Taken together, these results suggest that *LADON* has a pivotal role in regulating the expression of some players involved in the Rho/ROCK and Rac signalling pathways. Specifically, *LADON* appears to positively regulate the Rho/ROCK pathway and negatively influence the Rac-driven one, highlighting the potential function of *LADON* in balancing signal dynamics associated with cell migration and morphology (Fig.4 and Fig. 5).

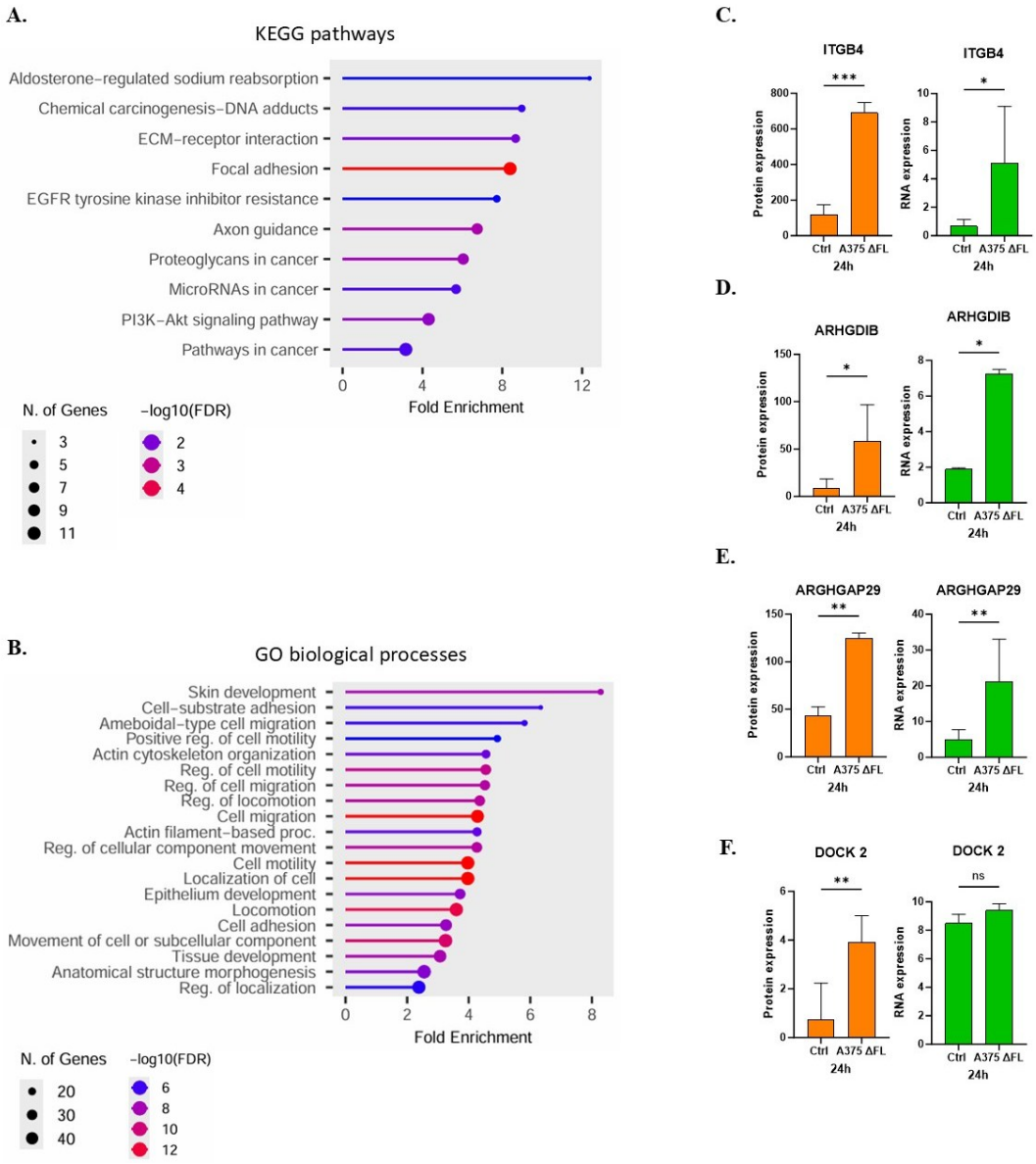

Figure 7. Proteomic analysis (control A375 vs A375ΔFL)

(**A**) Lollipop chart of the top-ranked KEGG pathways using as query genes those corresponding to proteins significantly downregulated (p-value < 0.05 and fold change < 0.66667) in unmodified A375 cells when compared to A375ΔFL at 48h. (**B**) Lollipop chart of the top-ranked GO biological process terms using as query genes those corresponding to proteins significantly downregulated (p-value < 0.05 and fold change < 0.66667) in unmodified A375 cells when compared to A375ΔFL at 48h.
RT-PCR with primers for ITGB4 (**C**), ARHGDIB (**D**), ARGHGAP29 (**E**) and DOCK2 (**F**) detecting the RNA expression at 24h of culture in A375ΔFL and control cells. RT-PCR histograms (in green) have been compared with histograms depicting the corresponding protein level of same factors (in orange).

For Lollipop graphs: fold enrichment is defined as the percentage of genes in the provided list that are in a that specific pathway. The number of enriched genes is represented by the size of the dot. P-values are calculated using the hypergeometric test, and false discovery rates (FDRs) are computed via the Benjamini-Hochberg method to

correct for multiple testing. While FDR measures statistical significance, fold enrichment indicates effect size. These diagrams were generated using a consistent significance threshold (p-value < 0.05), while applying different fold change cutoffs (> 1.5; between 0.5 and 1.5; or < 0.66667), as detailed in the main text. In Figure 7, we specifically focused on one of these fold change ranges (<0.66667) for illustrative purposes. Histograms display mean values ± SD. P-values were calculated in a Student's t test, * < 0.05, ** < 0.01, *** < 0.001.

LADON affects the expression of oncogenes and tumour suppressors

We focused on proteins that were identified by at least 3 independent peptides and with a significant (P<0.05) fold change superior to 1.5. These proteins are overexpressed in unmodified A375 cells and many of them turned out to be involved in tumour growth and metastasis promotion (RELB, RAB38, RAB7B) as shown in Table 2. In particular, RAB38 is a Small GTPases of the Ras oncogene family involved in intracellular trafficking, which has been reported to promote melanoma metastasis [24].

Conversely, among proteins that had a fold change inferior to 0.66667, we found several tumour suppressors (SORBS2/3, FOXP1, PML, TUSC1) that were significantly downregulated in unmodified A375 cells and so presumably repressed by *LADON*.

Taken together, these findings support previous observations [13] and suggest that the *LADON* transcript promotes the expression of oncogenes while repressing tumour suppressors involved in growth inhibition and metastasis control (Table 2).

Protein	Time (h)	(p) t-test	Fold Changes A375 Ctrl vs A375ΔFL	Function	Accession
Ras-related protein Rab-38 (RAB38)	24	0,000797772	1,800737327	Vescicle trafficking, melanoma metastasis and oncogenic activity	P57729
	48	0,00070233	1,610461056		
	72	0,003633148	1,608949804		
Ras-related protein Rab-7B (RAB7B)	24	0,000370737	1,707930726	Endosomal trafficking and oncogenic activity	Q96AH8
	48	0,000537855	2,007306366		
	72	0,018925737	1,912444039		
Transcription factor RelB (RelB)	24	0,033734075	1,768263574	Transcription regulation in NF-κB pathway, can acts as oncogene	Q01201
	48	×	×		
	72	×	×		
Protein PML	24	×	×	Key player in cellular senescence, tumor suppressor	P29590
	48	×	×		
	72	0,023759714	0,641860433		
Forkhead box protein P1 (FOXP1)	24	×	×	Transcription factor involved in tumor suppression	Q9H334
	48	0,025194661	0,087813831		
	72	0,044405303	0,108140541		
Sorbin and SH3 domain-containing protein 2 (SORBS2)	24	×	×	Tumor suppressor	O94875
	48	0,018492555	0,575683656		
	72	2,29473E-05	0,494418606		

Table 2. Some examples of presumably LADON-regulated oncogenes and tumour suppressors across all time points. Failure to detect a significant change of the protein level between A375 and A375ΔFL cells is marked with a cross.

LADON induced the expression of proteins involved in WNT signalling

Previous results suggested that *LADON* expression is positively regulated by WNT/β-CATENIN signalling in A375 cells [14]. A gene annotation analysis (Metascape) revealed an enrichment in the GO biological process "Wnt signalling pathway" (GO:0016055) with proteins that were found to be significantly ($P<0.05$) overexpressed (fold change superior to 1.5) in unmodified A375 cells compared to A375ΔFL cells. These proteins are involved in the canonical WNT/β-CATENIN signalling pathway (GSK3B, BCL9, SFRP1), including its positive regulation (DIXDC1, FRAT1), as well as in the promotion of Wnt protein secretion (WLS). Remarkably, most of these factors are significantly up-regulated in the control cell line only after 72h of culture, suggesting an indirect induction of them by *LADON*.

A noteworthy detail is that, whereas previous experiments performed in A375 cell line positioned *LADON* downstream of WNT/β-CATENIN signalling [14], the current proteomic analysis suggested a time-dependent induction of important players of this signalling pathway by *LADON*.

Finally, even if its comprehensive role in cancer progression is still under investigation, the activation of WNT signalling is reported to reduce melanoma proliferation [25], but also stimulates tumour cell invasion [26]. This fits with the results obtained in Fig. 3C, Fig. 3D, Fig. 4A and Fig. 4B.

LADON could affect the expression of translational regulators and play a role in the bioenergetic adaptation of melanoma cells

Despite amoeboid-moving cancer cells still retaining some actin-dependent steps of cell migration such as actin flow and actomyosin contractility, the energy demands resulting from strong adhesions and force transmission, stress fibers, cell–cell interactions, and proteolytic ECM remodelling are strongly reduced [21]. Indeed, it has been reported that low mitochondrial metabolism can induce rounded-amoeboid migration [27]. As a result, amoeboid-moving cancer cells rely on low mitochondrial activity and are hence considered to be energetically efficient [21].

A gene annotation analysis was performed to find proteins correlated to metabolic functions, some of which are summarized in Table 3. For this analysis we also considered proteins that were found to change slightly in their expression when comparing A375 control cells and A375ΔFL cells ($0.49 <$ fold change < 1.49, p-value < 0.05).

Among the annotated proteins, some of them were overexpressed (fold change superior to 1.5) in control A375 cells and turned out to be negative regulators of mitochondrial translation and ribosomal subunit biogenesis (MALSU1, GTBP2). Similarly, positive regulators of mitochondrial translation were found to be downregulated in the presence of *LADON* (MRPL17, MRRF, MRPL50,

RMND1). The mitochondrial genome encodes crucial proteins, mainly involved in the oxidative respiration [35]. Indeed, we found several proteins associated with the mitochondrial respiratory chain (UQCR1O, FASTKD3) and with the biogenesis of cytochrome c oxidase (COA6, COX15, TACO1, UQCC2) to be significantly repressed in the presence of *LADON*. Similarly, glycolytic proteins (PFKB4, SLC37A2, SLC16A3) were found to be downregulated in unmodified A375 cells. Since amoeboid dissemination of cancer cells can occur with very low energy consumption through the repression of oxidative respiration and glycolysis [21], these results are consistent with the potential amoeboid migration-inducing function of *LADON* in melanoma cells. Furthermore, some of the aforementioned proteins were found to be significantly differentially expressed at 48h, which we identified as a crucial time point for changes in the morphology of A375 cell (Fig. 5B).

Cancer cells must be able to adapt to environments that are deprived of energy. This is achieved by activating adaptive programs that enable escape from stressed regions and by downregulating highly energy-demanding processes, such as interactions with the extracellular matrix and, protein synthesis [21]. For instance, ENC1, PAIP2 and EIF4EBP1 are all three negative regulators of protein translation found to have a 1.3- to 1.5-fold increase in their expression in unmodified A375 cells.

Protein	Time (h)	(p) t-test	Fold Changes A375 Ctrl vs A375ΔFL	Function	Accession
MALSU1	24	×	×	GO:0070130 negative regulation of mitochondrial translation; GO:0090071 negative regulation of ribosome biogenesis	Q96EH3
	48	0,009818	1,615407461		
	72	×	×		
GTPBP2	24	×	×	Regulation of mitochondrial translation	Q9BX10
	48	0,00532	1,588532196		
	72	×	×		
MRPL50	24	×	×	GO:0032543 mitochondrial translation;GO:0140053 mitochondrial gene expression;GO:0006412 translation	Q8N5N7
	48	×	×		
	72	0,027229	0,512799654		
RMND1	24	×	×	GO:0070131 positive regulation of mitochondrial translation	Q9NWS8
	48	×	×		
	72	0,025063	0,807633723		
UQCR10	**24**	0,024018	0,613949818	Involved in the biogenesis of complex III of mitochondrial respiratory chain	Q9HD40
	48	×	×		
	72	×	×		
FASTKD3	**24**	0,019028	0,685126202	GO:0070131 positive regulation of mitochondrial translation; interacts with components of the mitochondrial respiratory chain	Q14CZ7
	48	×	×		
	72	×	×		
COA6	24	×	×	Biogenesis of cytochrome c oxidase (COX)	Q5JTJ3
	48	0,011847	0,638715822		
	72	×	×		
COX15	**24**	0,042363	0,876466698	Biogenesis of cytochrome c oxidase (COX)	Q7KZN9
	48	9,80E-05	0,6468166		
	72	0,026594	0,76250598		
PFKFB4	**24**	0,001059	0,721433188	Glycolytic protein that regulates the concentration of fructose-2,6-bisphosphate (F2,6BP)	Q16877
	48	0,001059	0,721433188		
	72	0,007574	0,666915985		
SLC37A2	24	0,013326	0,342938642	Glycolytic protein involved in the transport of glucose-6-phosphate and phosphate ions across the cell membrane	Q8TED4
	48	×	×		
	72	0,001225	0,28666208		

Table 3. Some examples of presumably LADON-regulated metabolic proteins. Failure to detect a significant change of the protein level between A375 and A375ΔFL cells is marked with a cross.

LADON 3' region might has a transcriptional repressive role (preliminary data)

To elucidate the role of *LADON*, it is essential to characterize that of its exon 2-flanking regions. Indeed, the regulatory motifs and elements within these sequences may provide valuable insights into *LADON*'s mode of action. Therefore, we used genome editing to delete the 3' region of this non-coding gene (Fig. 8). This allowed us to obtain several independent 3' region mutant clones, designated as A375ΔLAD3'. We focused on three of these clones, A375ΔLAD3'a to c, and characterized them using PCR (Fig. 9A).

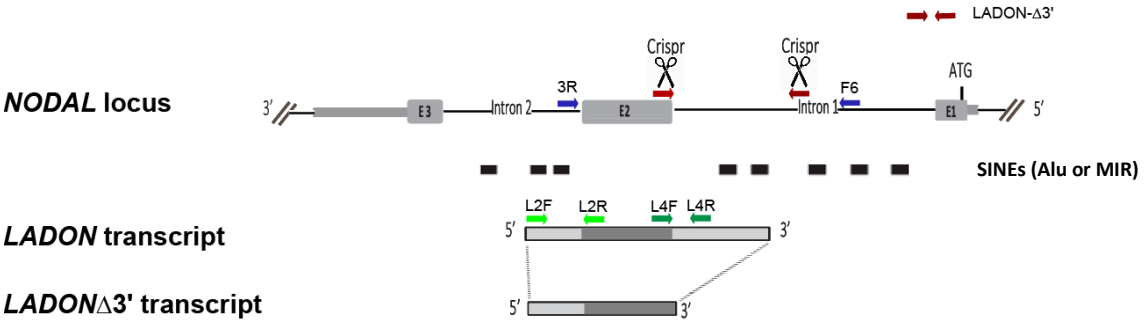

Figure 8. Diagram of *LADON* 3' region deletion and primers used.
Schematic of the human *NODAL* locus with its 3 exons (E1 to E3), showing the *LADON* transcript transcribed from the opposite strand below. The truncated *LADON*-Δ3' transcript is expressed in A375 cells deleted for the *LADON 3'*. The red arrows represent the oligos used to delete the 3' region (sequences in material and methods). 3R and F6 primers were used to identify the mutants through PCR. The arrows in green represent the primers used to track *LADON* transcript. The black boxes show the location of short interspersed nuclear elements (SINEs), primarily Alu and MIR sequences, some of which are missing in the *LADON*-Δ3' transcript.

The RT-qPCR analysis of *LADON* expression in A375ΔLAD3' cell mutants revealed a dramatic increase in its basal level (24h) compared to A375 control cells, implying that 3' region of *LADON* may exert a repressive effect on its own expression. Interestingly, similar to what was previously observed in A375ΔE2 mutants [13], *LADON* expression in A375ΔLAD3' clones did not increase significantly over time, suggesting that the deletion deprived *LADON* of a critical regulatory input (Fig. 9B).

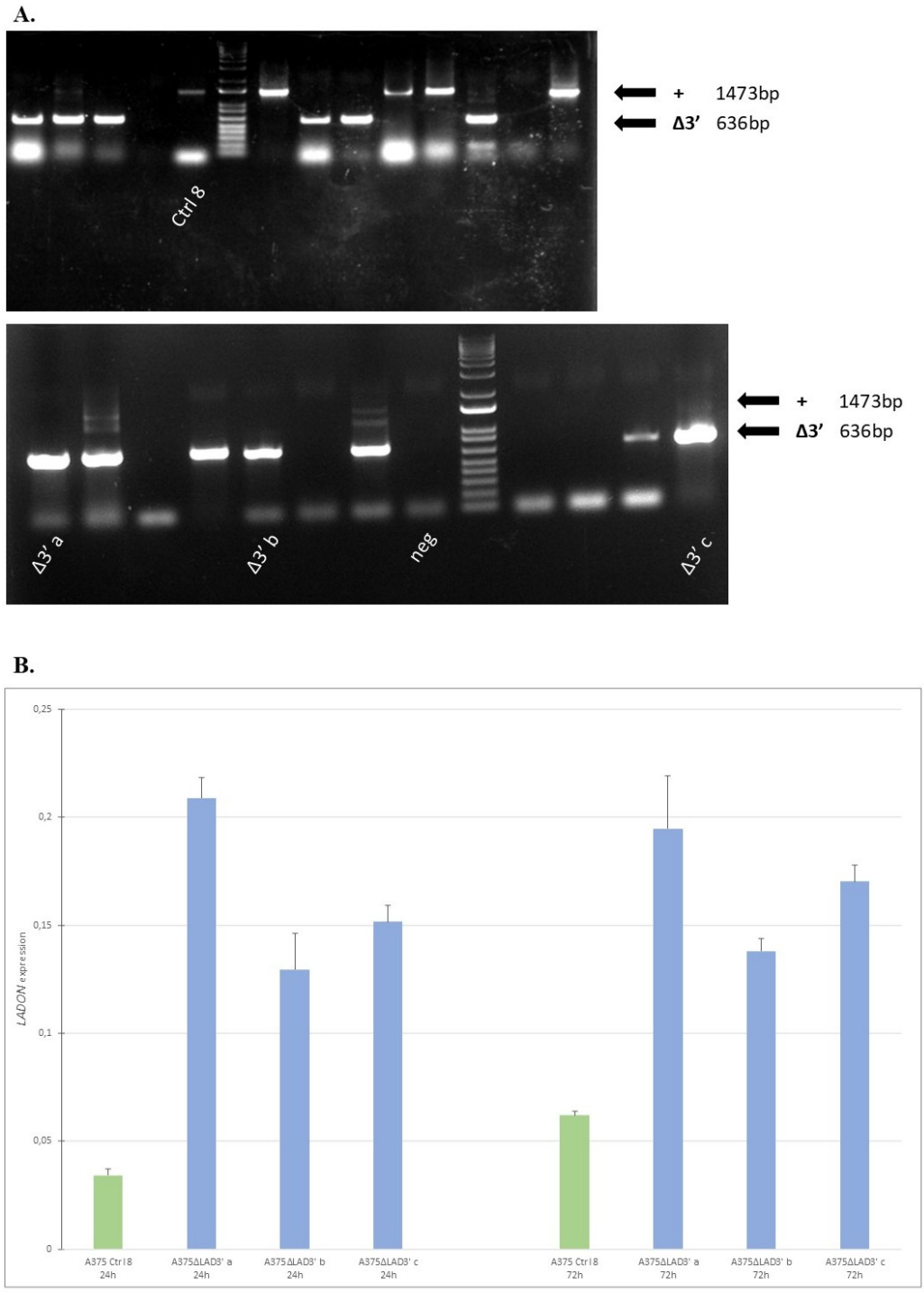

Figure 9. Identification of A375ΔLAD3' mutants and *LADON* expression analysis.

(A) PCR amplification with the 3R-F6 primer pair of the genomic region targeted by the CRIPSR/Cas9-mediated deletion of *LADON* 3' region in A375 cells. In the 24 independent clones analysed here (out of a total of 96), amplification of the intact locus yields a 1473bp-long band, while that of the deleted one (Δ3') yields a 636bp-long band. + and Δ3' indicate unmodified and 3' region-deleted clones respectively. **(B)** RT-PCR with primers (L2F and L2R) amplifying a region of 188 nt specific to *LADON* in three independent A375ΔLAD3' clones detects no increase over the course of the culture compared to A375 control.

Discussion

Although the precise mechanism of *LADON*'s action remains to be elucidated, its full-length deletion provided additional insights regarding the potential function of this lncRNA within the molecular network of melanoma growth progression and metastasis. Our findings showed that *LADON* has a significant impact on cell proliferation, cell morphology and cell migration of A375 cells, and in some cases the observed phenotypic defects were more severe than those originally characterized in exon 2-deleted cells, highlighting the importance of additional regions beyond the exon 2.

A375ΔFL cells exhibit a more proliferative phenotype rather than an invasive one when compared to controls or parental A375 cells (Fig. 3C, 3D). This is consistent with the current model used to describe melanoma cells, according to which invasive and proliferative identities correspond to two mutually exclusive transcriptional signatures. Melanoma cells can oscillate between these signatures during progression in response to specific microenvironmental cues [22]. We suppose that *LADON* could be involved in the switching of melanoma cells towards an invasive identity and that its absence forced the A375ΔFL cells to maintain a proliferative signature, which is more susceptible and less resistant to chemotherapy [22]. Furthermore, several studies highlighted the importance of the transcription factor MITF as a main regulator of melanoma proliferation [20,22]. Remarkably, MITF expression is required to maintain a proliferative signature [22]. Consistent with this, our proteomic analysis revealed that *LADON* significantly ($P<0.05$) downregulates (fold change inferior to 0.5) MITF expression after 24 hours in culture, providing a molecular insight for the reduced proliferative yet more invasive phenotype observed in A375 cells.

Although motile cells may use various strategies to move, the fundamental mechanisms by which they generate and transmit force appear to be remarkably conserved, with all animal cells, including cancer cells, relying on the dynamics of the actomyosin cytoskeleton, which is considered as the key generating force for migration [28]. RHO–GTPase/RHO-associated protein kinase (ROCK) signalling is the main regulator of cytoskeleton dynamics, defining different types of migration strategies, notably elongated/mesenchymal-type motility and rounded/amoeboid-type motility. Proteomic analysis and correspondent complementary RT-qPCR experiments showed a significant dysregulation of the expression of key players involved in Rho/ROCK and Rac1 signalling pathways, which we found to be positively and negatively regulated by *LADON*, respectively. The high actomyosin contractility that crucially characterizes amoeboid cells is driven by the ATPase function of the Myosin II regulatory light chains, which undergo phosphorylation through Rho/ROCK signalling. Previous Western blot analyses showed that A375ΔE2 cells expressed lower levels of phosphorylated myosin light chain 2 (pMCL2) [14], supporting our observations in A375ΔFL cells

and the hypothesis that *LADON* plays a pivotal role in positively regulating the Rho-ROCK-pMLC2-dependent amoeboid migration of melanoma cells. Interestingly, it has been reported that ROCK inhibition leads to a decrease in *LADON* expression [29] (referred to as *NODAL* in their qPCR array analysis). This implies that Rho/ROCK signalling, which operates downstream of *LADON*, may also play a role in promoting *LADON* expression.

The sustained Rho/ROCK signalling and the altered expression levels of components of the actin cytoskeleton, which are induced by the gradual increase of *LADON* expression, enhance rounded cell migration in A375 cells. *In vivo* measurements demonstrated that amoeboidal cell migration is 10-100 times more efficient than Rac-dependent elongated cell migration [21]. Indeed, our findings showed that the complete knockout of *LADON* in A375 melanoma cells results in a loss of their ability to adopt an amoeboid phenotype, leading to a drastic reduction in cell motility. Interestingly, at both 48h and 72h, the roundness index of A375ΔE2 cells is comparable with that of A375 and control cells (Fig. 5B, 5C), suggesting that only the full KO of *LADON* affects cell roundness and the conversion between mesenchymal and amoeboid modes of melanoma cells migration. These results highlight the functional relevance of *LADON*'s 5' and 3' regions and the potential involvement of Alu and MIR nuclear elements in regulating the mesenchymal to amoeboid transition (MAT). Another relevant aspect is that, even if A375ΔE2 clones display an amoeboid morphology similar to that of A375 cells, these mutants present a very low transmigration rate, comparable to that of A375ΔFL cells (Fig. 4A). This is probably because cell motility and invasive behaviour do not depend only on cell morphology, but also on other features, such as the degradation of the surrounding matrix through the secretion of matrix metalloproteases. Even if some amoeboid cells have been proposed to migrate without any matrix metalloprotease requirements [30], it has been reported that amoeboid melanoma cells invade via diffuse matrix degradation [31]. Another possible explanation is that the deletion of exon 2, as demonstrated in the Collignon team's previous study, deprived *LADON* of a critical regulatory input necessary to increase its expression over time, which appeared to correlate with the capacity of melanoma cell lines to acquire an invasive behaviour [13,14]. Therefore, the results shown in Fig. 4A suggest that the deletion of exon 2 is likely sufficient to drastically inhibit the invasive behaviour of A375 cells.

How *LADON* regulates the expression of its downstream effectors remains unclear, but the proteomic analysis conducted at three different time points provided some clues. A significant number of proteins (350-400 per time point) appeared to be targeted by the action of *LADON* across all time points (24, 48 and 72h), though fold change values differed (Fig. 6). This suggests that *LADON* likely acts as a dynamic regulator of A375 melanoma characteristics, initiating and maintaining a long-term proteomic remodelling over time. Some proteins were found to be significantly dysregulated by *LADON*'s absence only after 24h of culture (e.g.

MITF, ARHGDIB), suggesting that these factors could be early targets of the transcript. Based on phenotypic evidence (Fig. 5B) and the observation that a substantial number of factors involved in the mesenchymal-to-amoeboid transition are significantly regulated by *LADON* at the protein level specifically after 48 hours of culture, we propose that the 48h time point is critical for this transition. We hypothesize that at this point of the culture, the accumulation of specific physical and chemical cues could activate the potential *LADON* pathway, which would activate transcriptional programs involved in MAT, enhancing cell migration. Finally, some proteins were either down or up-regulated by *LADON* only after 72h of culture, suggesting that this regulation may not involve direct interaction between *LADON* and these proteins. Among these proteins, factors involved in WNT signalling were significantly induced.
In situ hybridization of *LADON* in induced pluripotent stem cells (iPSCs) provided additional insight into the potential mode of action of *LADON*. Using RNA probes against *LADON* in iPSCs allowed for the detection of a significant enrichment of the fluorescent *LADON* signal within the nucleus rather than the cytoplasm (results obtained in a parallel project in the Collignon Lab). A similar nuclear localization of the transcript was detected when using the same approach on a genetically engineered metastatic A375 cell line overexpressing a *LADON* transgene. Furthermore, LncATLAS (https://lncatlas.crg.eu/) is a web-based visualization platform that provides valuable information on the subcellular localization of long non-coding RNAs. According to LncATLAS, *LADON* (ENSG00000280401) predominantly localizes to the nucleus across the available cell lines in the database, including human embryonic stem cells (hESCs). According to these results, we could hypothesize that *LADON* acts at the nuclear level, thereby narrowing the range of mechanisms in which it might be involved (Fig. 1). Nevertheless, further experiments are necessary to confirm *LADON*'s localization (e.g. RNA-FISH using specific probes for *LADON*, RT-qPCR on nuclear vs. cytoplasmatic fractions), to evaluate whether this localization varies between different cell types, and to have a complete understanding of its molecular mechanism. Furthermore, additional experiments are required to validate proteomic data (e.g. Western blot analysis) and to better characterize cell morphological changes (e.g. confocal imaging).

To sum up (Fig. 10), *LADON* promotes a shift in metastatic melanoma cells toward a more invasive phenotype rather than a proliferative one. This is achieved through the upregulation of known oncogenes and the repression of tumour or metastasis suppressors. Notably, after 48h of culture, this regulatory activity results in reduced ECM-cell interactions (particularly integrin-mediated) and activated Rho/ROCK signalling. This leads to enhanced actomyosin contractility and the formation of highly propulsive membrane blebs. This highlights the role of *LADON* as a key intermediary in the mesenchymal-to-amoeboid transition of metastatic A375 melanoma cells, an essential driver of their invasiveness. The aggressiveness of amoeboid melanoma cells is attributed, in part, to the energetic efficiency of this

mode of migration [21,27]. Indeed, we believe that the expression of *LADON* also controls the bioenergetic signature of amoeboid-moving cancer cells by the inhibiting of mitochondrial activity. This results in reduced oxidative phosphorylation and glycolysis, which are both critical features of amoeboid cancer cells. Additional experiments are needed to demonstrate the potential mechanical link between *LADON* and mitochondrial dynamics, including mitochondrial fission and fusion. These processes have been reported to be closely associated with the interconversion between mesenchymal and amoeboid modes of migration [27].

We hypothesize that, in response to metabolic challenges, *LADON* plays a critical role in inducing low mechanical and bioenergetic complexity, allowing melanoma cells to migrate in an amoeboid manner, which is faster and more energy-efficient than any other reported mode of migration [21]. This enables the cells to survive and escape from energy-deprived or chemotherapy-compromised tissue environments. This hypothesis is supported by a previous *in vivo* result: histological analyses showed that primary tumours derived from mutant A375ΔE2 cells had a higher mitotic index but were also far more necrotic than those derived from unmodified cells [13]. The absence of *LADON* appears to have forced the metastatic melanoma cells to maintain a proliferative signature at the expense of their ability to adopt an invasive identity [22], eventually leading to nutrient and oxygen deprivation. Such conditions pose a significant challenge for rapidly growing tumours, such as melanoma, which have high energy requirements [21]. In the absence of *LADON*, mutant cells cannot escape from metabolically stressed environments to invade more favourable niches. They are also unable to adapt by lowering the energy consumption or downregulating energy-demanding processes such as ECM-cell interactions or protein translation. Consequently, melanoma mutant cells undergo necrosis, which highlights the pivotal role of *LADON* in the network of interactions that governs melanoma metastasis.

Sequence analysis of *LADON* revealed the presence of short interspersed nuclear elements (SINEs) Alu and MIR in its 5' and 3' exon 2-flanking regions, homologies to factors known for their role in development and cancer, and motifs associated with nuclear localization. Our results indicate that the complete knockout of *LADON* leads to distinct phenotypic changes and dysregulation of specific molecular players that are not observed in exon 2-deleted cells. Roundness measurements revealed the potential functional relevance of the exon 2-flanking regions, suggesting that the SINEs Alu and MIR play a critical role in the pro-metastatic activity of *LADON*. Published evidence demonstrating the functional relevance of such SINEs in the regulatory action of lncRNAs further supports this hypothesis [13,14]. Therefore, generating A375 cell lines mutated in either the 3' or 5' regions via genome editing is crucial to understanding their contribution to cell behaviour and gene expression. We recently showed that deletion of 3' region of *LADON* leads to an increase in its basal expression level compared to A375 control cells and to a loss of its ability to upregulate over time (Fig. 9B). Two

reasonable hypotheses could be raised: first, the 3' sequence might contribute to transcript destabilization, since the presence of Alu elements known to function as decay motifs through interactions with RNA-binding proteins [17]; second, the 3' genomic region may host cis-regulatory elements that normally act to supress or fine-tune its transcription. Further experiments are required to characterize and confirm the role of this region. In particular, given that both the deletion of *LADON*'s 3′ region and exon 2 [13] resulted in altered expression profiles, these findings suggest that the genomic locus of *LADON* may play a regulatory role, independently or in conjunction with its transcript. Therefore, a critical next step is to assess whether the regulatory effects of *LADON* are mediated by the transcript itself, the genomic DNA sequence or a combination of both. To address this, transcriptomics (RNA-seq) and epigenomics (ATAC-seq, CUT&TAG) analyses will provide a comprehensive view of how *LADON* influences gene expression and chromatin architecture. Specifically, by comparing different cellular conditions, A375 cells, full knockout and knockdown of the transcript, we will gain insights into the contribution of the *LADON* transcript versus its genomic sequence to its regulatory effects. Multi-omics data analyses can be complemented with rescue experiments of full knockout phenotype by re-expressing the transcript in A375ΔFL cells and evaluate its impact on cell migration, roundness and proliferation.

To conclude, we define a specific role for *LADON* within a regulatory network governing the invasive behaviour of melanoma cells (Fig. 10). This project also aims to point out the critical role of this transcript in defining the amoeboid features of melanoma cells, which turned out to be crucial for their aggressive behaviour, especially under challenging tumour microenvironments [19,21]. Amoeboid highly invasive melanoma cells exhibit cancer stem cell-like properties [29] and display immunosuppressive behaviour [32,33]. Moreover, they contribute significantly to therapy resistance and the formation of metastatic lesions [32,33,34]. Indeed, accumulating evidence indicates that amoeboid behaviour represents not only a mode of migration, but a distinct cellular state that cancer cells adopt to gain survival and invasive advantages [18,19,20,21]. In this context, *LADON* emerges as a promising therapeutic target for interventions aimed at impairing metastatic progression and enhancing melanoma treatment efficacy. Although previous findings strongly suggest that *LADON* functions independently of *NODAL* [13,14], analysis of publicly available datasets has revealed several cell types in which both genes are expressed. Co-expression of *NODAL* and *LADON* has been specifically confirmed in keratinocytes and induced pluripotent stem cells (iPSCs). Future investigations should therefore focus on the role of *LADON* in non-tumoral cells (such as the iPSCs), and in particular to investigate its possible involvement in the modulation of *NODAL* signalling for those cell types that express it. Furthermore, to better understand the role of *LADON* in metastatic melanoma and to assess its value as a potential target for therapeutic approaches, it will be necessary to study the role of *LADON* within the skin, the native cellular context where melanoma

tumours arise, grow and mature. The Collignon team recently started a collaboration with Jesús Lacal's team at the University of Salamanca to use an organotypic model of human skin based on the use of immortalized human keratinocytes. It will be possible then to generate skin models by mixing these keratinocytes with different melanoma cell lines, either expressing or lacking *LADON*. This ex-vivo model holds therefore a significant potential for investigating the pathophysiological functions of *LADON*.

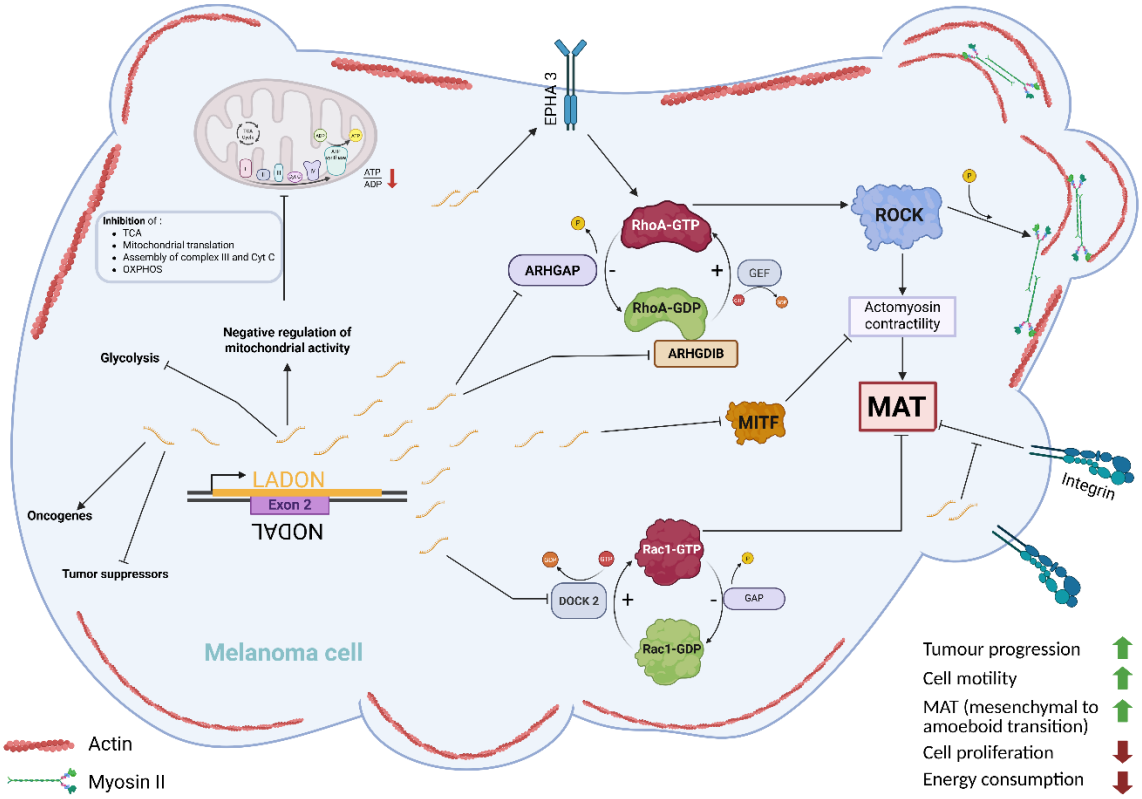

Figure 10. The potential role of *LADON*

Diagram showing key processes and regulatory pathways underlying the rounded-amoeboid mode of migration that are affected by the increase of *LADON* expression over a 4-day culture period in metastatic melanoma cells. The *LADON* transcript (depicted in yellow) promotes the transition from a proliferative cell identity to a less proliferative and more invasive cell identity. It promotes the expression of known oncogenes and represses that of tumour or metastasis suppressor, thereby modulating the expression of downstream targets, such as cytoskeleton components. Two main branches regulating rounded or elongated movement can be highlighted: the Rho/ROCK pathway, which promotes rounded–amoeboid invasion via myosin light chain II (MLC2) phosphorylation, and the Rac1 pathway, which drives elongated invasion. *LADON* inhibits Rac1 signalling by repressing the expression of DOCK2, a Rac1-specific guanine nucleotide exchange factor (GEF), resulting in the accumulation of inactive, GDP-bound Rac1. Conversely, *LADON* promotes the RhoA/ROCK signalling by repressing the expression of several GTPase-activating proteins (e.g. ARHGAP29, ARHGAP18 etc.) and Rho GDP-

dissociation inhibitor (ARHGDIB), facilitating the accumulation of the GTP-bound (active) state of RhoA GTPase, which is also promoted by the overexpression of Epha3. As a result, the actomyosin contractility of melanoma cells increase, leading to mesenchymal to amoeboid transition (MAT) that is critical to melanoma cell invasiveness. In parallel, *LADON* downregulates the expression of key factors involved in extracellular matrix (ECM)-cell interactions (particularly integrins) and components of focal adhesions, promoting the formation of plasma membrane blebs that further enhance amoeboid motility. Consistent with the bioenergetic profile of amoeboid cancer cells, *LADON* also represses mitochondrial activity, leading to reduced ATP production via oxidative phosphorylation (OXPHOS), thereby favouring a metabolically efficient migratory mode. Figure created with Biorender.com. Nucleus and cytoplasm are not showed in the schematic diagram for simplicity.

References

1. Huarte, M. (2015). The emerging role of lncRNAs in cancer. Nature Medicine, 21, 1253–1261. https://doi.org/10.1038/nm.3981
2. Neguembor, M. V., Jothi, M., & Gabellini, D. (2014). Long noncoding RNAs, emerging players in muscle differentiation and disease. Skeletal Muscle, 4, 8. https://doi.org/10.1186/2044-5040-4-8
3. Bonasio, R., & Shiekhattar, R. (2014). Regulation of transcription by long noncoding RNAs. Annual Review of Genetics, 48, 433–455. https://doi.org/10.1146/annurev-genet-120213-092323
4. Kretz, M., Siprashvili, Z., Chu, C., Webster, D. E., Zehnder, A., Qu, K., Lee, C. S., Flockhart, R. J., Groff, A. F., Chow, J., Johnston, D., Kim, G. E., Spitale, R. C., Flynn, R. A., Zheng, G. X. Y., Aiyer, S., Raj, A., Rinn, J. L., Chang, H. Y., & Khavari, P. A. (2013). Control of somatic tissue differentiation by the long non-coding RNA TINCR. Nature, 493(7431), 231–235. https://doi.org/10.1038/nature11661
5. Luo, H., Zhu, G., Xu, J., Lai, Q., Yan, B., Guo, Y., Zheng, Y., Liu, X., Hu, H., & Cai, H. (2019). HOTTIP lncRNA promotes hematopoietic stem cell self-renewal leading to AML-like disease in mice. Cancer Cell, 36(6), 645–659.e8. https://doi.org/10.1016/j.ccell.2019.10.011
6. Slaby, O., Laga, R., & Sedlacek, O. (2017). Therapeutic targeting of non-coding RNAs in cancer. Biochemical Journal, 474(24), 4219–4251. https://doi.org/10.1042/BCJ20170079
7. Strizzi, L., Hardy, K. M., Kirschmann, D. A., Ahrlund-Richter, L., & Hendrix, M. J. C. (2012). Nodal expression and detection in cancer: Experience and challenges. Cancer Research, 72(8), 1915–1920.
8. Bodenstine, T. M., Chandler, G. S., Seftor, R. E. B., Seftor, E. A., Gruman, L. M., & Hendrix, M. J. C. (2016). Plasticity underlies tumor progression: Role of Nodal signaling. Cancer and Metastasis Reviews, 35(1), 21–39. https://doi.org/10.1007/s10555-016-9605-5
9. Bianco, C., Adkins, H. B., Wechselberger, C., Seno, M., Normanno, N., De Luca, A., Sun, Y., Khan, N., Kenney, N., Ebert, A., & Salomon, D. S. (2002). Cripto-1 activates Nodal- and ALK4-dependent and -independent signaling pathways in mammary epithelial cells. Molecular and Cellular Biology, 22(8), 2586–2597.
10. Papageorgiou, I., Nicholls, P. K., Wang, F., Lackmann, M., Makanji, Y., Salamonsen, L. A., Robertson, D. M., & Harrison, C. A. (2009). Expression of Nodal signalling components in cycling human endometrium and in endometrial cancer. Reproductive Biology and Endocrinology, 7, 122. https://doi.org/10.1186/1477-7827-7-122
11. Topczewska, J. M., Postovit, L.-M., Margaryan, N. V., Sam, A., Hess, A. R., Wheaton, W. W., Nickoloff, B. J., Topczewski, J., & Hendrix, M. J. C. (2006). Embryonic and tumorigenic pathways converge via Nodal signaling: Role in melanoma aggressiveness. Nature Medicine, 12(8), 925–932. https://doi.org/10.1038/nm1431

12. Findlay, S. D., & Postovit, L. M. (2018). Comprehensive characterization of transcript diversity at the human NODAL locus. bioRxiv, 254409. https://doi.org/10.1101/254409
13. Dutriaux, A., Diazzi, S., Bresesti, C., Hardouin, S., Deshayes, F., Collignon, J., & Flagiello, D. (2023). LADON, a natural antisense transcript of NODAL, promotes tumour progression and metastasis in melanoma. Non-Coding RNA, 9(6), 71. https://doi.org/10.3390/ncrna9060071
14. Dutriaux, A., Diazzi, S., Caburet, S., Bresesti, C., Hardouin, S., Deshayes, F., Collignon, J., & Flagiello, D. (2020). LADON, a natural antisense transcript of NODAL, promotes the acquisition of an invasive behaviour in melanoma cells. bioRxiv. https://doi.org/10.1101/2020.04.09.032375
15. Hruz, T., Laule, O., Szabo, G., Wessendorp, F., Bleuler, S., Oertle, L., Widmayer, P., Gruissem, W., & Zimmermann, P. (2008). Genevestigator V3: A reference expression database for the meta-analysis of transcriptomes. Advances in Bioinformatics, 2008, 420747. https://doi.org/10.1155/2008/420747
16. Wu, J., Jiang, J., Chen, B., Wang, K., Tang, Y., & Liang, X. (2021). Plasticity of cancer cell invasion: Patterns and mechanisms. Translational Oncology, 14(1), 100899. https://doi.org/10.1016/j.tranon.2020.100899
17. Gong, C., & Maquat, L. E. (2011). lncRNAs transactivate STAU1-mediated mRNA decay by duplexing with 3′ UTRs via Alu elements. Nature, 470(7333), 284–288. https://doi.org/10.1038/nature09701
18. Barzegar Behrooz, A., & Shojaei, S. (2024). Mechanistic insights into mesenchymal–amoeboid transition as an intelligent cellular adaptation in cancer metastasis and resistance. Biochimica et Biophysica Acta (BBA) - Molecular Basis of Disease, 1870(7), 167332. https://doi.org/10.1016/j.bbadis.2024.167332
19. Graziani, V., Rodriguez-Hernandez, I., Maiques, O., & Sanz-Moreno, V. (2022). The amoeboid state as part of the epithelial-to-mesenchymal transition programme. Trends in Cell Biology, 32(3), 228–242. https://doi.org/10.1016/j.tcb.2021.10.004
20. Orgaz, J. L., & Sanz-Moreno, V. (2013). Emerging molecular targets in melanoma invasion and metastasis. Pigment Cell & Melanoma Research, 26(1), 39–57. https://doi.org/10.1111/pcmr.12041
21. Parlani, M., Jorgez, C., & Friedl, P. (2023). Plasticity of cancer invasion and energy metabolism. Trends in Cell Biology, 33(5), 388–402. https://doi.org/10.1016/j.tcb.2022.09.009
22. Keith S. Hoek, Ossia M. Eichhoff, Natalie C. Schlegel, Udo Döbbeling, Nikita Kobert, Leo Schaerer, Silvio Hemmi, Reinhard Dummer; In vivo Switching of Human Melanoma Cells between Proliferative and Invasive States. Cancer Res 1 February 2008; 68 (3): 650–656. https://doi.org/10.1158/0008-5472.CAN-07-2491
23. Lawrenson, I. D., Wimmer-Kleikamp, S. H., Lock, P., Schoenwaelder, S. M., Down, M., Boyd, A. W., Alewood, P. F., & Lackmann, M. (2002). Ephrin-A5 induces rounding, blebbing and de-adhesion of EphA3-expressing 293T and melanoma cells by CrkII. Journal of Cell Science, 115(6), 1059–1072.
24. Huang, M., Qi, T. F., Li, L., Zhang, G., & Wang, Y. (2018). A targeted quantitative proteomic approach assesses the reprogramming of small GTPases

during melanoma metastasis. Cancer Research, 78(18), 5431–5445. https://doi.org/10.1158/0008-5472.CAN-18-0461
25. Biechele, T. L., Kulikauskas, R. M., Toroni, R. A., Lucero, O. M., Reyna, D., James, R. G., Robin, N. C., Dawson, D. W., Moon, R. T., & Chien, A. J. (2012). Wnt/β-catenin signaling and AXIN1 regulate apoptosis mediated by inhibition of BRAFV600E kinase in human melanoma. Science Signaling, 5(206), ra126. https://doi.org/10.1126/scisignal.2002274
26. Grossmann, A. H., Yoo, J. H., Clancy, J., Sorensen, L. K., Sedgwick, A., Tong, Z., Ostanin, K., Rogers, A., Grossmann, K. F., Tripp, S. R., Thomas, K. R., D'Souza-Schorey, C., Odelberg, S. J., & Li, D. Y. (2013). The small GTPase ARF6 stimulates β-catenin transcriptional activity during WNT5A-mediated melanoma invasion and metastasis. Science Signaling, 6(265), ra14. https://doi.org/10.1126/scisignal.2003398
27. Crosas-Molist, E., Bertran, E., Sancho, A., Barbany-Cairó, J., Egea, J., Hernández-Losa, J., & Fabra, Á. (2021). AMPK is a mechano-metabolic sensor linking cell adhesion and mitochondrial dynamics to myosin II-dependent cell migration. Developmental Cell. Advance online publication. https://doi.org/10.2139/ssrn.3845005
28. Yamada, K. M., & Sixt, M. (2019). Mechanisms of 3D cell migration. Nature Reviews Molecular Cell Biology, 20, 738–752. https://doi.org/10.1038/s41580-019-0172-9
29. Rodriguez-Hernandez, I., Maiques, O., Kohlhammer, L., et al. (2020). WNT11-FZD7-DAAM1 signalling supports tumour initiating abilities and melanoma amoeboid invasion. Nature Communications, 11, 5315. https://doi.org/10.1038/s41467-020-18951-2
30. Wolf, K., Müller, R., Borgmann, S., Bröcker, E.-B., & Friedl, P. (2003). Amoeboid shape change and contact guidance: T-lymphocyte crawling through fibrillar collagen is independent of matrix remodeling by MMPs and other proteases. Blood, 102(9), 3262–3269. https://doi.org/10.1182/blood-2002-12-3791
31. Orgaz, J., Pandya, P., Dalmeida, R., et al. (2014). Diverse matrix metalloproteinase functions regulate cancer amoeboid migration. Nature Communications, 5, 4255. https://doi.org/10.1038/ncomms5255
32. Georgouli, M., Herraiz, C., Crosas-Molist, E., Fanshawe, B., Maiques, O., Perdrix, A., Pandya, P., Rodriguez-Hernandez, I., Ilieva, K. M., Cantelli, G., Karagiannis, P., Mele, S., Lam, H., Josephs, D. H., Matias-Guiu, X., Marti, R. M., Nestle, F. O., Orgaz, J. L., Malanchi, I., Fruhwirth, G. O., Karagiannis, S. N., & Sanz-Moreno, V. (2019). Regional activation of Myosin II in cancer cells drives tumor progression via a secretory cross-talk with the immune microenvironment. Cell, 176(4), 757–774.e23. https://doi.org/10.1016/j.cell.2018.12.038
33. Orgaz, J. L., Crosas-Molist, E., Sadok, A., Perdrix-Rosell, A., Maiques, O., Rodriguez-Hernandez, I., Monger, J., Mele, S., Georgouli, M., Bridgeman, V., Karagiannis, P., Lee, R., Pandya, P., Boehme, L., Wallberg, F., Tape, C., Karagiannis, S. N., Malanchi, I., & Sanz-Moreno, V. (2020). Myosin II reactivation and cytoskeletal remodeling as a hallmark and a vulnerability in

melanoma therapy resistance. Cancer Cell, 37(1), 85–103.e9. https://doi.org/10.1016/j.ccell.2019.12.003

34. Cantelli, G., Orgaz, J. L., Rodriguez-Hernandez, I., Karagiannis, P., Maiques, O., Matias-Guiu, X., Nestle, F. O., Marti, R. M., Karagiannis, S. N., & Sanz-Moreno, V. (2015). TGF-β-induced transcription sustains amoeboid melanoma migration and dissemination. Current Biology, 25(22), 2899–2914. https://doi.org/10.1016/j.cub.2015.09.054
35. Amorim, A., Fernandes, T., & Taveira, N. (2019). Mitochondrial DNA in human identification: a review. PeerJ, 7, e7314. https://doi.org/10.7717/peerj.7314